Unclassified

SECURITY CLASSIFICATION OF THIS PAGE

REPORT DOCUMENTATION PAGE

Form Approved OMB No. 0704-0188

1a. REPORT SECURITY CLASSIFICATION
Unclassified

1b. RESTRICTIVE MARKINGS

2a. SECURITY CLASSIFICATION AUTHORITY

2b. DECLASSIFICATION / DOWNGRADING SCHEDULE

3. DISTRIBUTION / AVAILABILITY OF REPORT
Approved for public release; distribution is unlimited.

4. PERFORMING ORGANIZATION REPORT NUMBER(S)
BRL-TR-2863

5. MONITORING ORGANIZATION REPORT NUMBER(S)

6a. NAME OF PERFORMING ORGANIZATION
Ballistic Research Laboratory

6b. OFFICE SYMBOL (If applicable)
SLCBR-TB-B

7a. NAME OF MONITORING ORGANIZATION

6c. ADDRESS (City, State, and ZIP Code)
Aberdeen Proving Ground, MD 21005-5066

7b. ADDRESS (City, State, and ZIP Code)

8a. NAME OF FUNDING / SPONSORING ORGANIZATION
USA Harry Diamond Laboratories

8b. OFFICE SYMBOL (If applicable)
SLCHD-NW

9. PROCUREMENT INSTRUMENT IDENTIFICATION NUMBER

8c. ADDRESS (City, State, and ZIP Code)
2800 Powder Mill Road
Adelphi, MD 20783-1197

10. SOURCE OF FUNDING NUMBERS

PROGRAM ELEMENT NO.	PROJECT NO.	TASK NO.	WORK UNIT ACCESSION NO.
62120A	1L162120AH25		

11. TITLE (Include Security Classification)
Buckling of Blast Loaded Cylinder

12. PERSONAL AUTHOR(S)
Santiago, Joseph M., Klaus*, Michael H, and Wisniewski, Hank L.

13a. TYPE OF REPORT
Final

13b. TIME COVERED
FROM FY85 TO FY86

14. DATE OF REPORT (Year, Month, Day)

15. PAGE COUNT
65

16. SUPPLEMENTARY NOTATION *Mr. Klaus was employed by the NBC Protection Research and Development Institute of the Federal Republic of Germany during the time he participated in this investigation under the auspices of the US/GE Scientist and Engineer Exchange Program - Group 42(1984).

17. COSATI CODES

FIELD	GROUP	SUB-GROUP
	13	13
	15	06

18. SUBJECT TERMS (Continue on reverse if necessary and identify by block number)
Dynamic Buckling Analysis; Thin-Walled Cylinder; Air Blast Loading; Nuclear Blast Survivability; Shock Wave Envelopment; Finite Element Analysis; Shell Finite Elements; Correlation of Strain Histories

19. ABSTRACT (Continue on reverse if necessary and identify by block number)

The transient response of a thin-walled aluminum cylinder subjected to an enveloping shock wave has been simulated with the ADINA finite element program and the results have been compared with counterpart experimental data. The analysis employed the ADINA 16-noded rectangular curved shell. Using a linear analysis, the computed strain histories at gage locations were found to correlate reasonably well with test records for the first four milliseconds, but some strain records rapidly diverged thereafter. A subsequent nonlinear analysis showed dynamic buckling to be the principal cause of this discrepancy. The nonlinear calculations and test results were found to generally agree in the number of buckling nodes, the magnitude of the deformation, and frequencies excited, although buckling sensitivity to imperfections prevented an exact coincidence of circumferential modes.

20. DISTRIBUTION / AVAILABILITY OF ABSTRACT
☒ UNCLASSIFIED/UNLIMITED ☐ SAME AS RPT. ☐ DTIC USERS

21. ABSTRACT SECURITY CLASSIFICATION
Unclassified

22a. NAME OF RESPONSIBLE INDIVIDUAL
Joseph M. Santiago

22b. TELEPHONE (Include Area Code)
(301) 278-6042

22c. OFFICE SYMBOL
SLCBR-TB-B

DD Form 1473, JUN 86 — Previous editions are obsolete. — SECURITY CLASSIFICATION OF THIS PAGE

18. SUBJECT TERMS (Continued):

Comparison of Experiment and Analysis
Shell Eigen-Frequencies
Frequency Analysis

AD

TECHNICAL REPORT BRL-TR-2863

BUCKLING OF BLAST LOADED CYLINDER

JOSEPH M. SANTIAGO
MICHAEL H. KLAUS
HENRY L. WISNIEWSKI

OCTOBER 1987

US ARMY BALLISTIC RESEARCH LABORATORY
ABERDEEN PROVING GROUND, MARYLAND

DESTRUCTION NOTICE

Destroy this report when it is no longer needed. DO NOT return it to the originator.

Additional copies of this report may be obtained from the National Technical Information Service, U.S. Department of Commerce, Springfield, VA 22161.

The findings of this report are not to be construed as an official Department of the Army position, unless so designated by other authorized documents.

The use of trade names or manufacturers' names in this report does not constitute indorsement of any commercial product.

TABLE OF CONTENTS

LIST OF ILLUSTRATIONS

I. INTRODUCTION

The transient response of a thin-walled aluminum cylinder subjected to an enveloping shock wave has been simulated with the ADINA finite element program and the results have been compared with counterpart experimental data. The analysis employed the ADINA 16-noded rectangular curved shell element. Using a linear analysis, the computed strain histories at gage locations were found to correlate reasonably well with test records for the first 4 milliseconds, but some strain records rapidly diverged thereafter. A subsequent nonlinear analysis showed dynamic buckling to be the principal cause of this discrepancy. The nonlinear calculations and test results were found to generally agree in the number of buckling nodes, the magnitude of the deformation, and frequencies excited, although buckling sensitivity to imperfections prevented an exact coincidence of circumferential modes.

II. BACKGROUND

This report presents a comparison between a finite element analysis of the transient response of a thin-walled aluminum cylinder to an enveloping blast wave and the test results from a counterpart experiment. The commercially available ADINA[1] computer program was used for this study because of the variety of transient response solution methods at its disposal. This work is part of an effort to investigate the susceptibility of lightweight structures to the combined thermal/blast effects of nuclear explosions and to assess the capabilities of finite element programs in accurately predicting the resulting structural response.

The basis for the comparison is series of tests performed by Pearson, et al[2], in 1980 in which cylinder specimens were exposed in the BRL 2.2 meter shock tube to a blast only, thermal only, and a combined thermal/blast loading. Thin-walled cylinders were chosen as representative of the lightweight construction typical of missile and airframe bays. During each test, a cylinder, with both ends clamped, was positioned with its axis perpendicular to the direction of the blast wave and/or thermal radiation. By maintaining the intensities of the blast and thermal loadings constant for the series of tests, a synergistic effect was conclusively demonstrated, in that the response to the combined thermal/blast loading was significantly greater than the responses to the individual loadings.

In 1982, Gregory and Pearson[3] attempted to reproduce the experimental results using solid brick elements in the ADINA program to model the cylinder, but the comparison with measured deflections was not very good. At the time, the poor correlation was attributed to an excessive distortional stiffness caused by the use of single brick elements through the shell thickness, although no attempt had been made to compare with the strain gage records. Never-the-less, this first attempt did suggest that perhaps an element more suitable to modeling thin-walled structures would perform better. For this reason, the present analysis employed shell elements.

This investigation concentrated on selecting an appropriate element to model the thin-walled aluminum cylinder of the experiment and on evaluating the performance of the resulting model against the blast only results. One reason the blast only test was chosen as a basis of comparison was that, of the three loading combinations, its loading and response records were the cleanest and most complete. More specifically, detailed transient blast loading data had been collected and, in addition to the final deformed configuration being measured, a substantial number of strain gages had been employed to record the transient response. A second reason for the choice was that the successful modeling of this simplest case would provide a sound basis for modeling the more complex thermal loading cases. Moreover, a study of the test results obtained by Pearson, et al[2], showed that even this case displays many of the complex characteristics, such as buckling, that became more prominent in the other two cases. In other words, continuation of the study would hinge on successfully modeling the blast only case.

III. CYLINDER SPECIFICATIONS

The test involved exposing a thin-walled cylinder to a blast wave generated in the BRL 2.2 meters diameter shock tube[4]. The cylinder was positioned in the test section of the shock tube with its axis perpendicular to that of the shock tube, so that the blast wave enveloped the cylinder circumferentially. The test specimen was manufactured from a rectangular sheet of 6061-T6 aluminum that was rolled into a cylinder and butt welded along the seam. During the test, care was taken to have this seam facing away from the direction of maximum load intensity. To achieve the clamped edge boundary conditions, strap clamps were used to fix the two ends of the cylinder onto two relatively rigid steel cylinders, which, in turn were attached to the test fixture so as to prevent the relative motion of the two ends.

The specimen dimensions were:

$$\begin{aligned} L &= \text{length between clamped ends} &&= 0.8 \text{ m} &&(31.5 \text{ in.}) \\ D &= \text{inside diameter} &&= 0.3048 \text{ m} &&(12.0 \text{ in.}) \\ h &= \text{wall thickness} &&= 1.016 \text{ mm} &&(0.04 \text{ in.}) \end{aligned}$$

giving a D/h ratio of 300, well within thin shell theory. The mechanical properties as obtained from a tensile test were:

$$\begin{aligned} E &= \text{Young's modulus} &&= 64.73 \text{ GPa} &&(9388 \text{ kpi}) \\ \nu &= \text{Poisson's ratio} &&= 0.3285 && \\ & \text{yield stress} &&= 301 \text{ MPa} &&(43.7 \text{ kpi}) \\ & \text{yield strain} &&= 0.4195\ \% && \\ & \text{plastic tangent modulus} &&= 650 \text{ MPa} &&(94.3 \text{ kpi}) \end{aligned}$$

The mass density was taken as the nominal value for aluminum at 55 degrees Celsius:

$$\rho = \text{density} = 2700 \text{ kg/m}^3 \ (5.24 \text{ slug/ft}^3)$$

IV. FINITE ELEMENT MODEL

The finite element model of the cylinder is depicted in Fig. 1. The figure illustrates the global coordinates and the local basis vectors employed. By taking advantage of the symmetry of the structure and the assumed symmetry of the applied loads, only a quarter of the cylinder had to be modeled. This was accomplished by placing symmetry planes through the cylinder axis and perpendicular to the axis midway from the clamped ends. Hence, only one clamped boundary was modeled, the upper boundary in Fig. 1.

The ADINA curved shell element with 16 mid-surface nodes[5] was employed, with 6 elements in the axial direction and 12 elements in the circumferential direction, resulting in a 72 element modeling with 703 nodes. The choice of 12 elements in the circumferential direction was dictated by the location of the pressure transducers at 15 degree intervals on the upper test fixture cylinder. In this way, the element boundaries were made to coincide with locations at which pressure histories were experimentally measured. In setting up the problem, it was necessary to not only specify the nodal coordinates, but also to define the initial directions of the normals to the cylinder, V_n, at the 37 circumferential nodal stations, as illustrated.

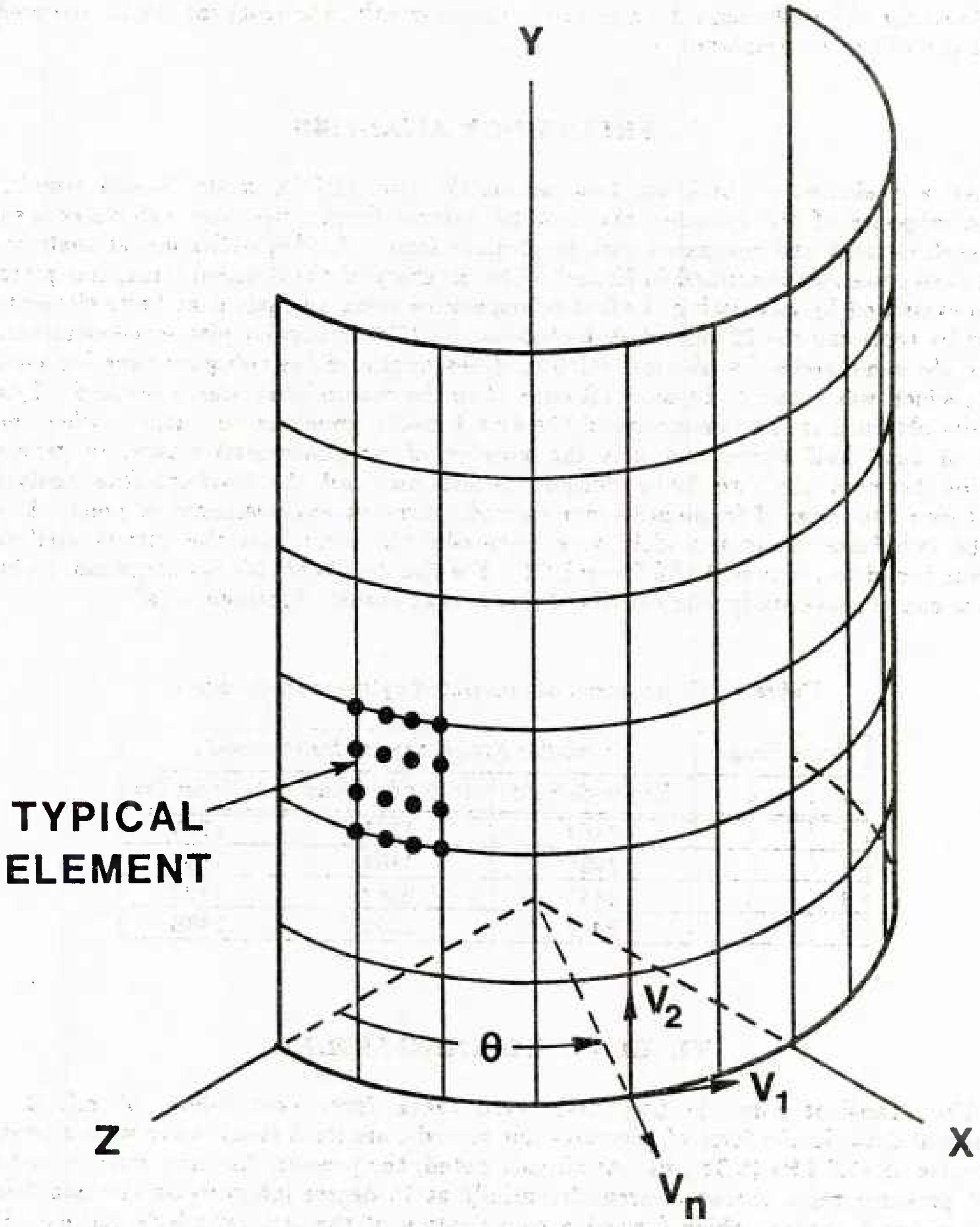

Figure 1. ADINA finite element model of one quarter of the cylinder using 16-noded shell elements.

Boundary conditions were specified by limiting the degrees-of-freedom (DOF) along the boundaries: on the z-x symmetry plane no displacements in the y direction and no rotations about the V_1 direction, on the y-z symmetry plane no displacements in the x direction and no rotations about the V_2 direction, and on the clamped edge no displacements or rotations at all. Moreover, rotation about the normal vector, V_n, were disregarded at all nodes because this DOF is undefined for the shell element employed[5]. Consequently, the resulting model required 3184 DOF for the 703 nodes employed.

V. FREQUENCY ANALYSIS

As a preliminary check on how accurately the ADINA model would simulate the transient response of the cylinder, the first 20 natural frequencies were calculated using the curved shell element and compared with predictions from a Rayleigh-Ritz modal analysis of the Donnell shell equations described in Kraus[6]. The accuracy of the 3-noded triangular plate-shell[7] was also evaluated by calculating the first 6 frequencies using an equivalent finite element model obtained by replacing the 72 curved shell elements by 1296 triangular plate-shell elements, while retaining the same nodal distribution. Both analyses employed the subspace iteration method of solution, which was found to be more effective than the determinant search method. Typical of the results obtained is the comparison of the first 4 modes presented in Table 1, where m is the number of axial half waves and n is the number of circumferential waves. In general, the correlation between the two finite element calculations and the Rayleigh-Ritz analysis was excellent over the range of frequencies investigated. From an engineering view point, the results using the two finite element models were essentially the same, but the curved shell element model was found to required 16 % fewer DOF. For the details of this investigation, including a numerical convergence study, the interested reader may consult Santiago, et al[8].

Table 1. Comparison of computed cylinder frequencies.

Mode Shape		Circular Frequency (radian/second)		
m	n	Rayleigh-Ritz	16-Node Quad	3-Node Tri
1	4	1804	1775	1745
1	5	1902	1894	1862
1	6	2443	2464	2422
1	3	2451	2395	2338

VI. BLAST LOADING MODEL

The transient blast loading data were taken from shot 8-80-7 of ref. 2. These experimental data, in the form of pressure-time records, are for a shock wave with a peak static overpressure of 43.7 kPa (6.34 psi). As already noted, the pressure histories were recorded by a series of pressure gages mounted circumferentially at 15 degree intervals on the non-deforming upper cylindrical fixture, which formed a continuation of the test cylinder's surface. For the purpose of the present analysis, the pressure history at each circumferential location was assumed to apply to the entire cylinder generator. In other words, the spatial distribution of the pressure on the cylinder was assumed to vary only circumferentially and to be uniform in the axial direction. Moreover, since the gages were rigidly mounted, coupling between loading

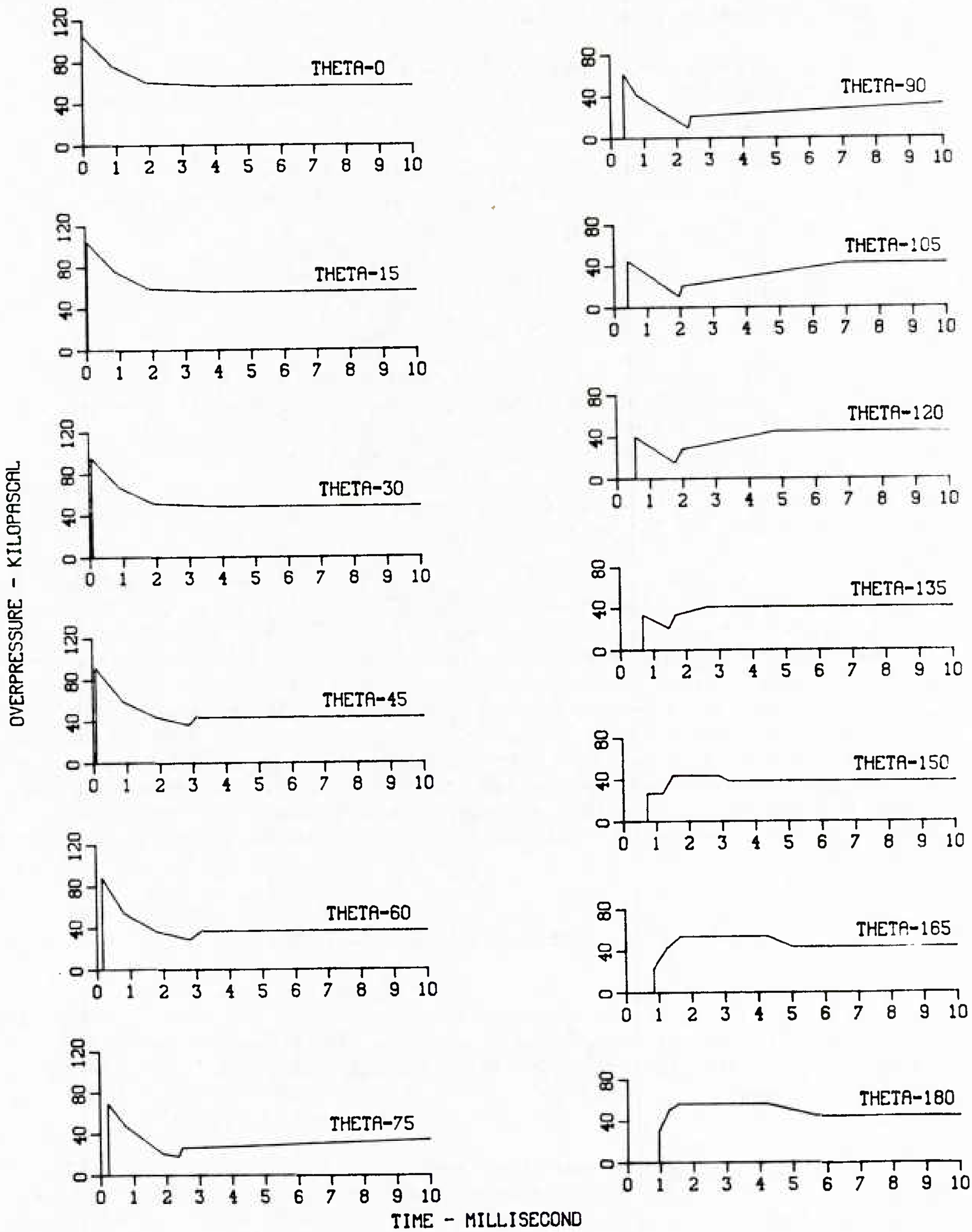

Figure 2. Pressure-time loading functions derived from experimental data recorded at circumferential stations.

and deflection of the specimen could not be taken into account, but this effect can be presumed negligible for the relatively small deflections involved.

The pressure-time records were digitized for the first 10 milliseconds as piece-wise linear histories, as illustrated by Fig. 2. Some of the more prominent fluid dynamical features displayed by these graphs are:

- The increased delay in the arrival time of the shock front as the angle θ increases, with a maximum of 0.95 milliseconds at 180 degrees.

- The overpressure at the face-on location (zero degrees) decaying from 105 kPa normal reflected pressure to 54.4 kPa stagnation pressure.

- The secondary rise in the pressure which emanates from the back of the cylinder (detectable in the graphs from 45 to 150 degrees) caused by the shock fronts on each side of the cylinder meeting at the 180 degree location and proceeding to re-envelop the cylinder.

For more details on the shock envelopment process, the reader is directed to the excellent pictorial description in Fig. 5 of ref. 2.

As alluded to earlier, the ADINA program accepts pressure histories defined at the corner nodes of each element and linearly interpolates the corner values over the element in order to calculate the equivalent nodal forces. The interpolation is accomplished by defining over each set of four elements sharing a common node a pyramid function that assumes the value of the node pressure at the apex node and that vanishes at the corner nodes. The pressure over an element is then easily found by summing the contributions from the pyramid functions at the four corner nodes. This procedure is illustrated in Fig. 3 for the present (two-dimensional) case, in which dash lines represent the pyramid functions defined for each corner node and the solid line represents the full pressure acting on each element, obtained by summing the contributions from the corner node pyramid functions. The program then uses the resultant pressure to compute the equivalent forces at all nodes, both corner and interior, in a consistent manner.

VII. STRAIN CALCULATIONS

In performing an analysis, the ADINA program computes strains at the Gauss integration points of each element. However, only the values at the corner Gauss points are easily retrievable for comparison with experimental data. The present analysis used the default values of $3 \times 3 \times 2$ for the Gauss point distribution associated with each 16-noded shell element, resulting in the distribution depicted in Fig. 4, wherein cell coordinates are used to specify point locations and the open circles denote the points at which strain values are saved.

During the experiment, a total of ten strain gages placed on the inner surface of the cylinder were used to record transient strain histories. Fig. 5 shows the locations and directions of these gages superimposed on a developed projection of the finite element model. This figure assumes the symmetric deformation of the cylinder, and, hence does not distinguish between gage locations on the upper or lower and left or right quarters of the cylinder. The precise locations of these gages in terms of the axial distance from the mid-plane and circumferential angle are presented in Table 2.

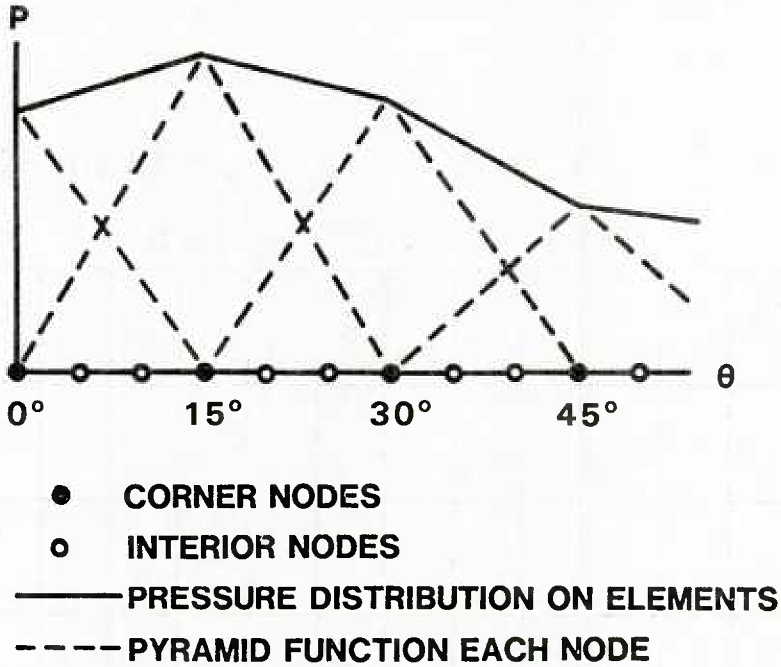

Figure 3. Generation of the pressure over the interior of an element by a linear interpolation of the pressure functions defined at corner nodes.

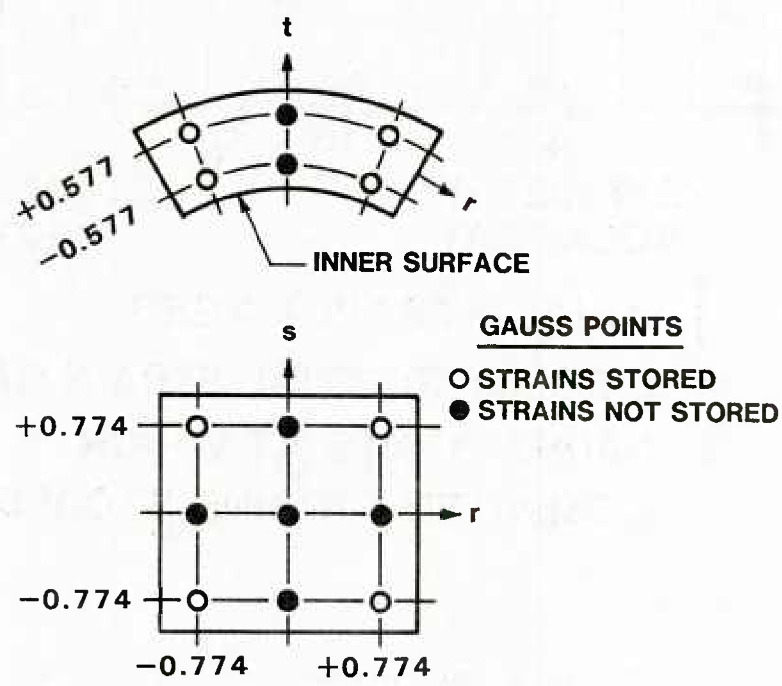

Figure 4. Location of the Gauss integration points employed in a typical 16-noded shell element.

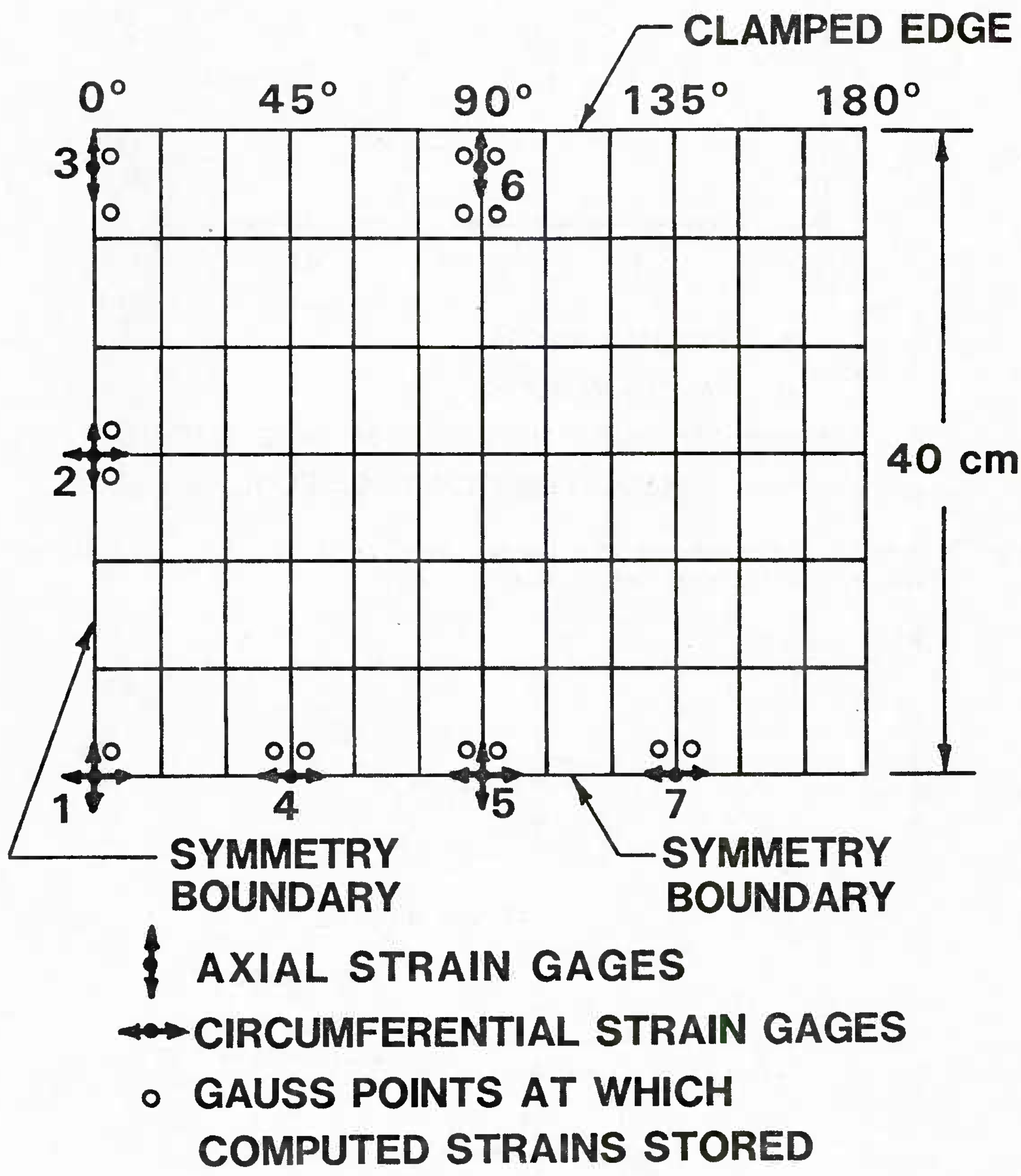

Figure 5. Geometric locations and orientations of the strain gages on the cylinder and the locations of the adjacent Gauss points used for interpolation.

Table 2. Locations of strain gages on test cylinder.

Gage number	Gage direction	Angle from face-on position (degree)	Distance from mid-plane (cm)
1	axial & circ.	0	0.0
2	axial & circ.	0	19.7
3	axial	0	-37.5
4	circumferential	315	0.0
5	axial & circ.	270	0.0
6	axial	270	-37.5
7	circumferential	135	0.0

Since the gages recorded strains at the inner surface, while the program computed strains at Gauss points located in the shell interior (see Fig. 4), it was necessary to linearly extrapolate interior values along the normal or t direction to the inner surface. Moreover, as Fig. 5 makes clear, the geometric locations of the gages do not coincide with the Gauss integration points at which the computed strains were stored, so that some manipulation of the computed values was required to compare with experimental records. This was accomplished by a simple linear interpolation of the strain values computed at the adjacent Gauss points; Fig. 5 shows the Gauss points adjacent to each gage location as open circles. Notice that only two Gauss points were required for gage locations on the symmetry boundaries and only one for those at the intersection of symmetry boundaries, since there are mirror image Gauss points symmetrically located outside the boundaries.

Because the program calculates strain components relative to global xyz coordinates, see Fig. 1, rather than shell tangent coordinates, a transformation was necessary in order to obtain components in the gage directions at some locations. For the axial strains at gage locations 1, 2, 3, 5 and 6 in Fig. 5, no transformations were required, since they are given directly by the e_{yy} components. Neither were transformations of the circumferential strains at gage locations 1 and 2 necessary, since they are considered sufficiently well approximated by e_{xx}, nor for that at gage location 5 since e_{zz} is sufficiently close there. Only at gage locations 4 and 7 were transformations necessary in order to determine the circumferential strains. The transformation was accomplished easily by applying Mohr's circle formula[9]:

$$e_{cir} = \frac{1}{2}\left[e_{zz} + e_{xx} - (e_{zz} - e_{xx})\cos 2\theta - e_{xz}\sin 2\theta\right] \tag{1}$$

where θ is the angle between the z-axis and the normal vector, see Fig. 1. The circumferential strains at locations 4 and 7 were then obtained by simply substituting 45 and 135 degrees for θ in this formula.

In actuality, it was found more effective to program the above procedure in somewhat reverse order:

- First, where necessary, (1) transformed the strain components at the Gauss points adjacent to gage locations of interest to circumferential strains.

- Second, strain values at all Gauss points neighboring gage locations were extrapolated to the inner surface.

- Third, the just computed surface values adjacent to each gage location were interpolated to obtain the computed values of the strains in the appropriate directions (axial or circumferential) at the gage locations.

In addition to permitting the computed strains to be compared with the experimental strains, this procedure provided some degree of smoothing of the strains across element boundaries.

VIII. LINEAR ANALYSIS

A linear analysis was first performed to determine the strain history at each gage location for comparison with the experimental records. The elastic material properties, summarized in Chapter III, were read in as initial input data. The loading was supplied at each time step from the pressure histories as described in Chapter VI. As in the frequency analysis, a consistent mass matrix formulation was employed. The implicit (Newmark) time integration method was used with $a = 0.25$ and $b = 0.5$, (the so-called trapezoid rule). The calculation proceeded for 200 time steps using an increment of 50 microseconds, for a total real time of 10 milliseconds.

The increment of 50 microseconds, chosen for convenience, was sufficiently small to adequately model the first 20 vibratory modes predicted by the frequency analysis, since the highest mode calculated had a period of 847 microseconds. Moreover, the test records, Fig. 6 and 7, indicate that the period of the dominant response frequency was in the order of 1.7 milliseconds, more than an order of magnitude greater than the time increment.

The comparison between computed strain histories and the experimental records is shown in Fig. 6 and 7. The data compare rather well for the axially oriented gages (Fig. 6). For instance, the comparisons of frequencies at locations 5 and 6, as well as the first 4 to 5 ms at location 1, show excellent agreement. Only a sight phase shift is apparent, which can be attributed to stiffening due to the use of a consistent mass formulation, see Strang and Fix[10]. Moreover, except at location 3 and the last 5 milliseconds at location 1, relative differences in the amplitudes are very small.

It is interesting to contrast the correlations obtained at the two gage locations near the boundary; while that at location 6 is excellent, the one at location 3 is not as good. This implies that the clamped edge condition was satisfied better at the location side-on to the blast wave than at the face-on location, where some slipping may have occurred. This is not too surprising, since the face-on location received the full brunt of the reflected pressure and, hence, the edge is more apt to slip there.

The comparisons between the computed and recorded strain histories in the circumferential direction are noticeably poorer (Fig. 7). Even during initial times, frequencies do not correlate nearly as well. Moreover, with the exception of location 4, the experimental records begin to diverge noticeably from the computed results after 3 to 5 milliseconds. Though not as pronounced, this unusual behavior can also be detected in the axial histories at locations 1 and possibly 3, although the erratic correlation at the latter location makes a definitive statement difficult. The records of the circumferential strains along the mid-section of the cylinder (locations 1, 4, 5, and 7) imply that the divergent behavior may be associated with a pattern of circumferential waves, suggesting, perhaps, that some buckling has occurred. This conjecture is confirmed somewhat by the noticeably smaller effect on the axial records. To explore the possibility of buckling using ADINA, a nonlinear analysis was necessary.

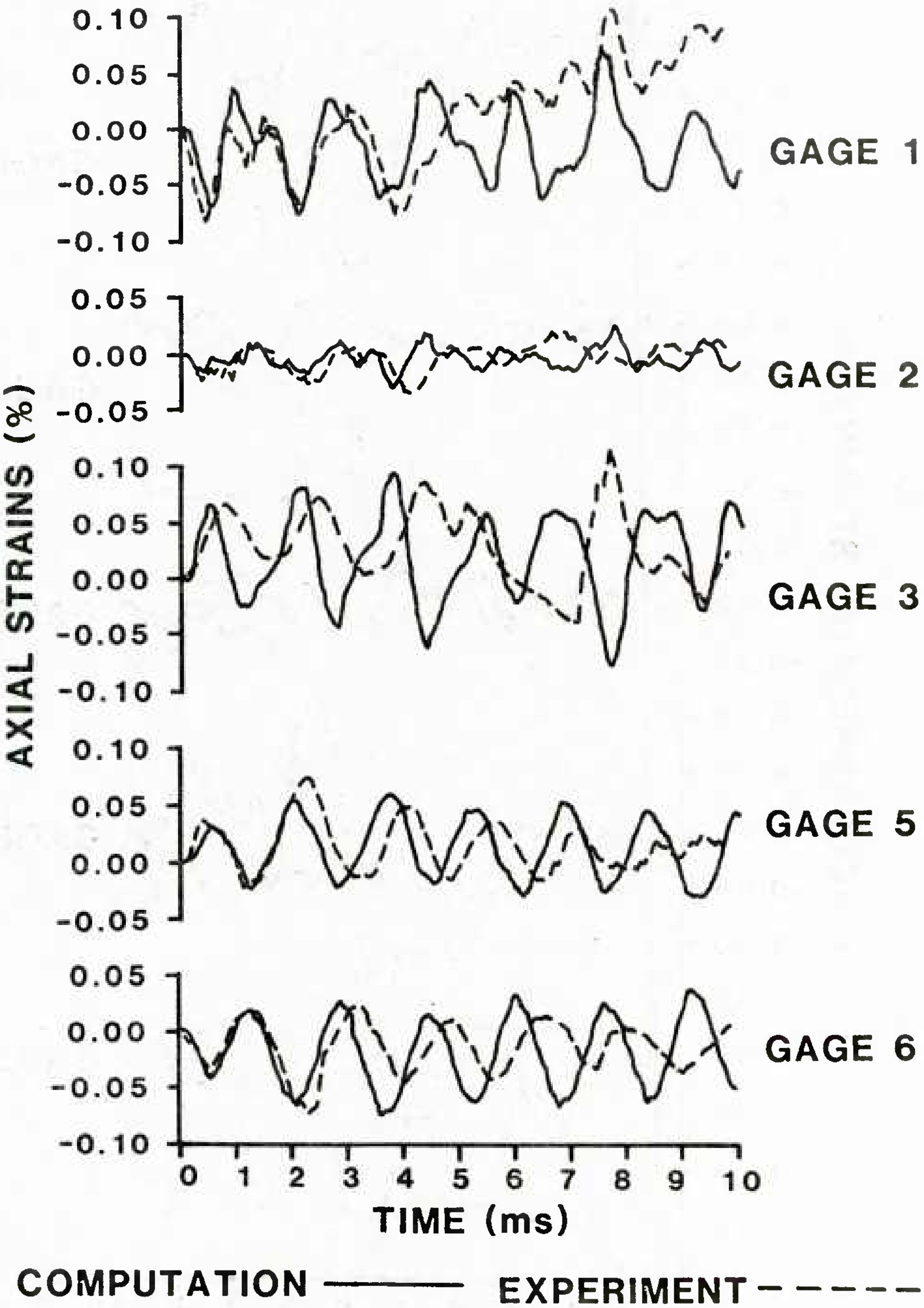

Figure 6. Comparison of linearly computed and experimental strain histories at axially oriented gage locations.

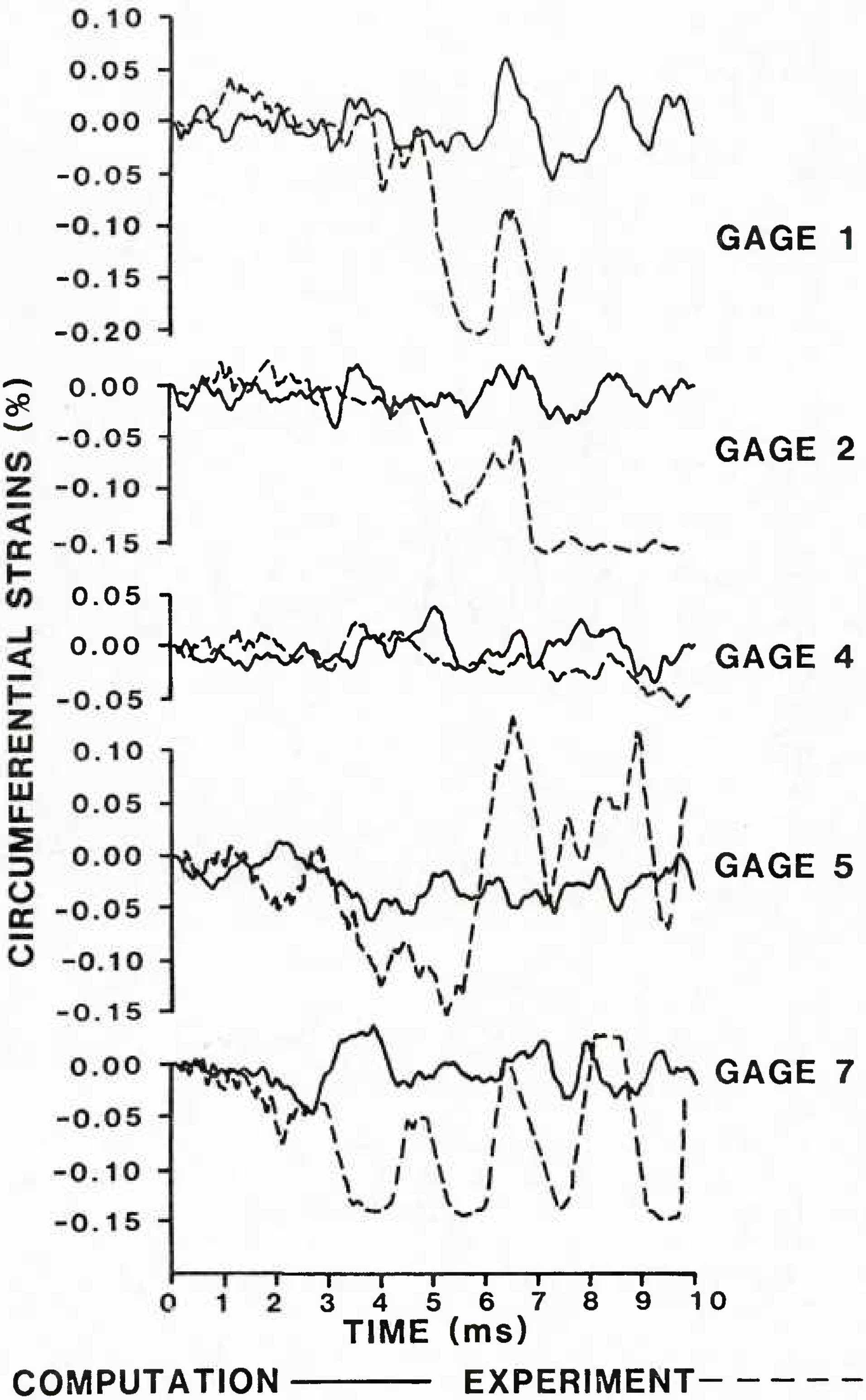

Figure 7. Comparison of linearly computed and experimental strain histories at circumferentially oriented gage locations.

IX. BUCKLING LOAD CALCULATION

As a first step the critical buckling pressure and corresponding mode shape were determined using the von Mises equation[11] for a cylinder subjected to a uniform external pressure:

$$P_{cr} = \frac{hE}{a}\left\{\frac{K^2}{n^2-1} + \frac{1}{12(1-\nu^2)}\left(\frac{h}{a}\right)^2\left[n^2-1+(2n^2-1-\nu)K\right]\right\} \tag{2}$$

$$K = \frac{1}{1+(nL/\pi a)^2} \tag{3}$$

where a (= .1529 m) is the mean radius of the cylinder, n is the number of circumferential waves, and the other parameters have been previously defined in Chapter III. Although this equation applies strictly to hinged boundary conditions only, because the length to radius ratio is greater than 5, the boundaries can be considered remote enough to allow its application to clamped edge boundaries. Substituting the values for the test cylinder in this expression yields a threshold pressure of 42 kPa for an associated buckling mode with 4 circumferential waves.

Although the experimentally measured pressures, as shown in Fig. 2, are not spatially uniform, we do observe that the pressures at the first three stations decay to approximately 60 kPa after their initial peaks of approximately 100kPa, while those at the remaining stations hover at about 40 kPa. Hence, the experimental pressures can be expected to induce buckling, the average clearly being in the range of the predicted critical buckling pressure. Moreover, if the buckling did indeed occur dynamically, the theory of dynamic buckling would predict that mode shapes corresponding to the locally higher pressures are more likely to be observed[12]. Solving (2) and (3) for the next higher modes, we find a pressure of 47 kPa corresponding to 5 circumferential wave and 65 kPa corresponding to 6 circumferential waves, well within the range of the experimentally observed pressures and implying that 5 and possibly even 6 circumferential waves can be expected to occur. The post test measurement of the cylinder cross-section, Fig. 8, appears to verify that possibility, implying that perhaps five circumferential waves were involved.

X. NONLINEAR ANALYSIS

With this evidence that the cylinder may have experienced some buckling, a geometric nonlinear transient analysis was undertaken with the same loading functions as used in the linear analysis. The nonlinear analysis employed the total Lagrangian formulation available with the shell element. As in the linear analysis, the trapezoid rule was used for implicit time integration, with the same time step of 50 microseconds. However, it was necessary to use a lumped mass matrix, rather than a consistent mass matrix, because only the former option has been programmed into the nonlinear solution algorithm for the curved shell element. Hence, the nonlinear analysis was not the exact analog of the linear case.

The results of the nonlinear analysis confirmed to a great extent that buckling had taken place. Indeed, the circumferential strain histories computed at 15 degree intervals along the inner surface at the mid-cylinder circumference, as shown in Fig. 9, reveal a significant increase in their amplitudes beginning at approximately 4 milliseconds, corresponding to the onset of buckling experimentally observed in the strain gage records. The computed mid-cylinder radial

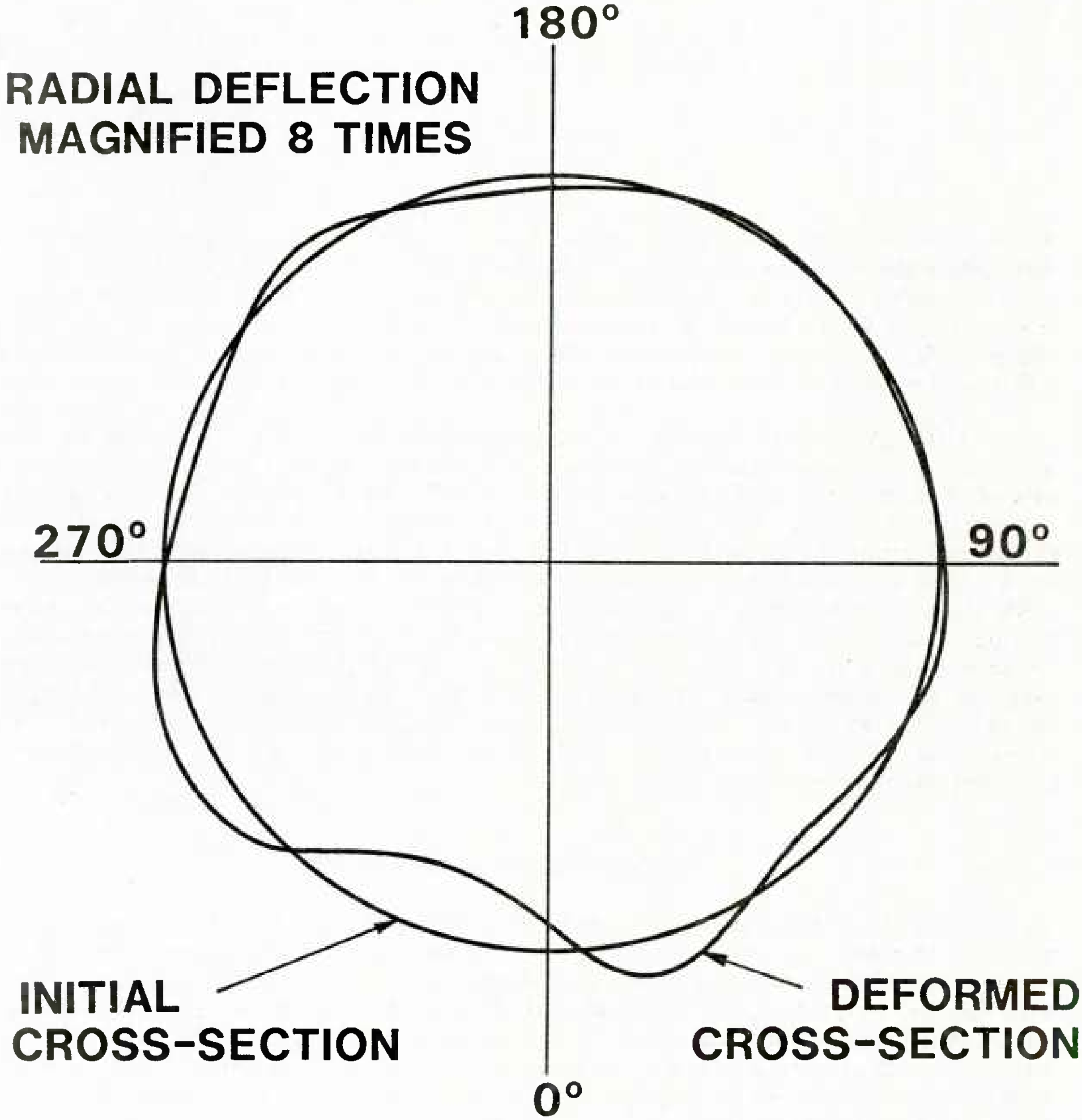

Figure 8. Post test measurements of the mid-cylinder radial deflection.

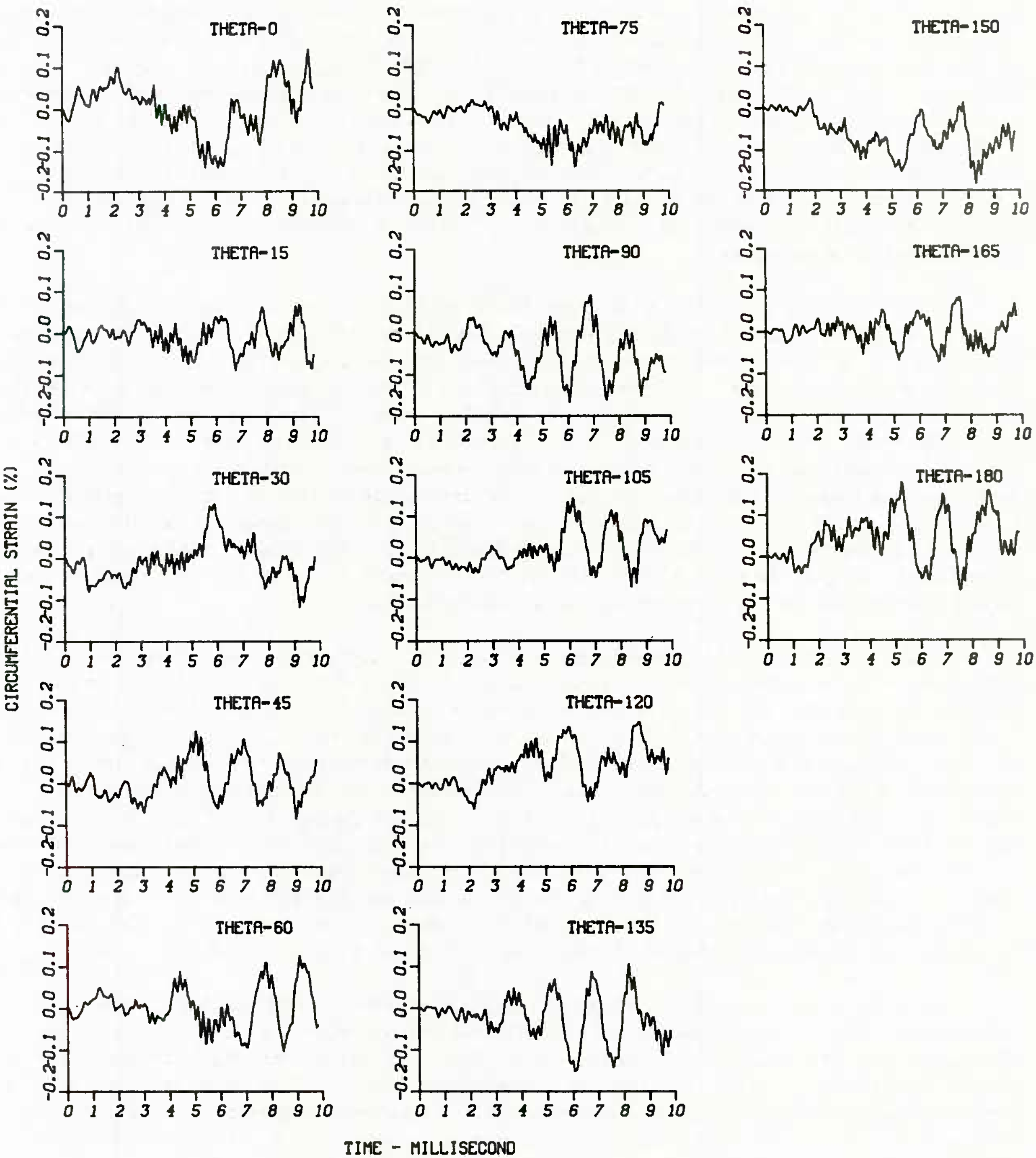

Figure 9. Circumferential strain histories computed from the nonlinear solution on the inner surface at mid-cylinder stations 15 degree apart.

deflections, depicted in Fig. 10, corroborate the last result by also exhibiting a noticeable increase after 4 milliseconds. Moreover, the deflected cross-sections, despite some erratic oscillations, indicate a fairly persistent pattern of five circumferential waves, with the locations of the maxima and minima remaining fairly stationary, in agreement with dynamic buckling theory and the experimental post-shot shape (Fig. 8). Isometric computer plots of the deformed surface of the cylinder, collected at select times in the appendix at the end of this report, also verify the occurrence of dynamic buckling. As is to be expected, they show that the deformation is considerably more complex than predicted by the buckling analysis. For example, from these plots we see how the longitudinal deformation progessively becomes more complex with time: starting as a single wave and by 6 millisecond beginning to show the development of three waves.

When the computed strain histories are directly compared with the corresponding test data for the strain gages along the mid-cylinder, Fig. 11 and 12, the correlations are not entirely satisfactory. The computed histories for the axially oriented gages (Fig. 11), though somewhat choppier than those from the linear solution (Fig. 6), are in general agreement with these computations and compare reasonably well with test results. The computed histories for the circumferentially oriented gages (Fig. 12), although an improvement over the linear solutions (Fig. 7) in clearly simulating the increase in amplitudes following buckling, do not correlate that well with test results at all gage locations. For example, the computed strains at gage locations 1, 5, and 7 are certainly a considerable improvement over the linearly computed strains in modeling the magnitude and frequency during buckling, but the general trends are not exactly reproduced. At gage location 4 the linear analysis is clearly closer to the test result, since the gage did not record an increased strain accompanying buckling.

On the other hand, considering the lack of exactitude that occurs in buckling phenomena due to uncertainties in loading and material properties, we thought it worthwhile to attempt to compare the test records with the computed strains at other circumferential locations in order to improve the correlation, as depicted in Fig. 13. Except at gage 5, where the best correlation is still obtained with the strains computed at 90 degrees, we notice an immediate improvement in the correlations. For example, the correlations between the gage 1 record and the computed history at 135 degree, and the gage 4 record and the 15 degrees history show considerable improvement over those in Fig. 12. And, indeed, the correlation between the gage 7 record and the 150 degrees history is extraordinarily good. Ideally, it would have been more convincing if a consistent (and hopefully small) rotation of the computed strain stations about the cylinder axis had resulted in an improved correlation at all the strain gage locations, but, despite a number of attempts, no such rotation was discovered.

It is important to point out that the computed strains, in agreement with experimentally observations (Fig. 7), never exceeded the plastic yield strain, implying that at least for the first 10 milliseconds only elastic buckling has taken place. To make sure that the use of a purely elastic analysis was valid, an additional geometric and material nonlinear analysis was performed and was found to give identical results. The elastic behavior of the deformation to some extent explains the oscillation observable in Fig. 9, since there was no plastic dissipation to absorb the kinetic energy and, hence, "freeze" the buckled pattern.

However, the conclusion that only elastic deformation took place, does somewhat conflict with the post-test measurement of permanent deformation in the cross-section, Fig. 8. Accepting that plastic yielding most likely occurred after 10 milliseconds, there is the question of what caused this to happen. Possible causes are:

- Intial imperfections in the geometry of the test specimen (a certain amount of out-of-roundness was detected in specimens[2]).

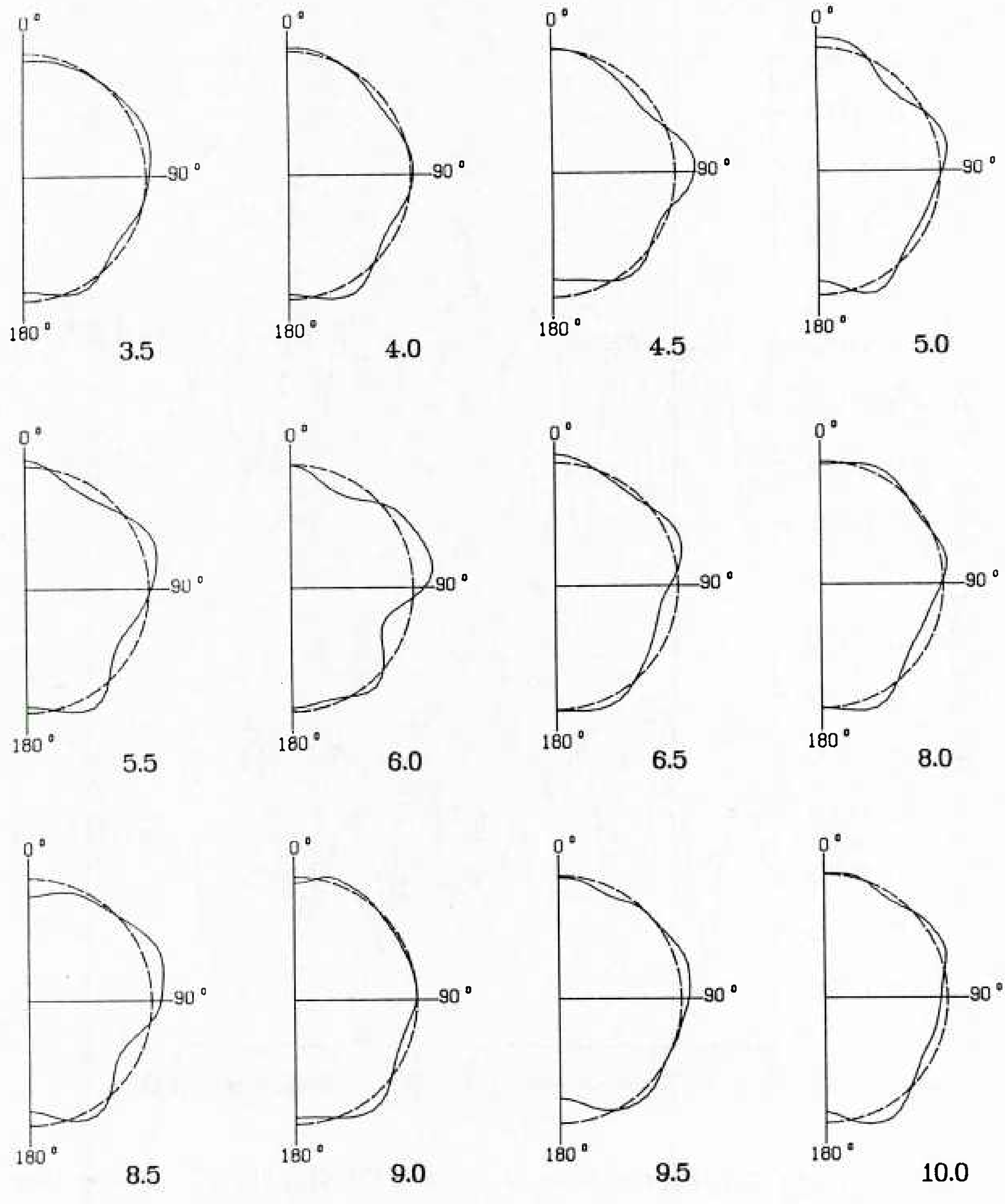

Figure 10. Deflection pattern of the mid-cylinder cross-section at select times (in milliseconds) as computed by the nonlinear analysis.

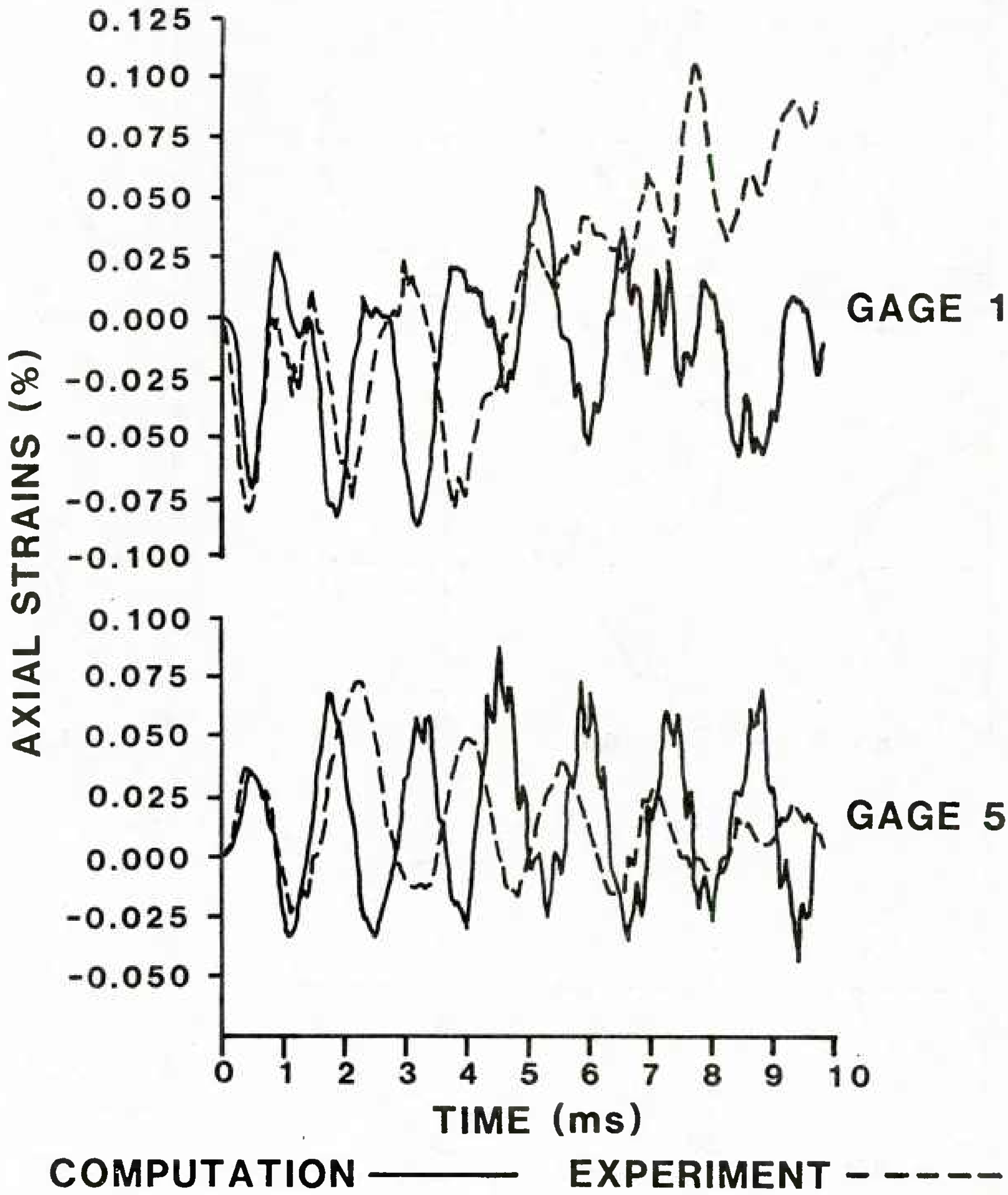

Figure 11. Comparison of axial strain histories recorded at mid-cylinder gage locations and computed by the nonlinear analysis at corresponding stations.

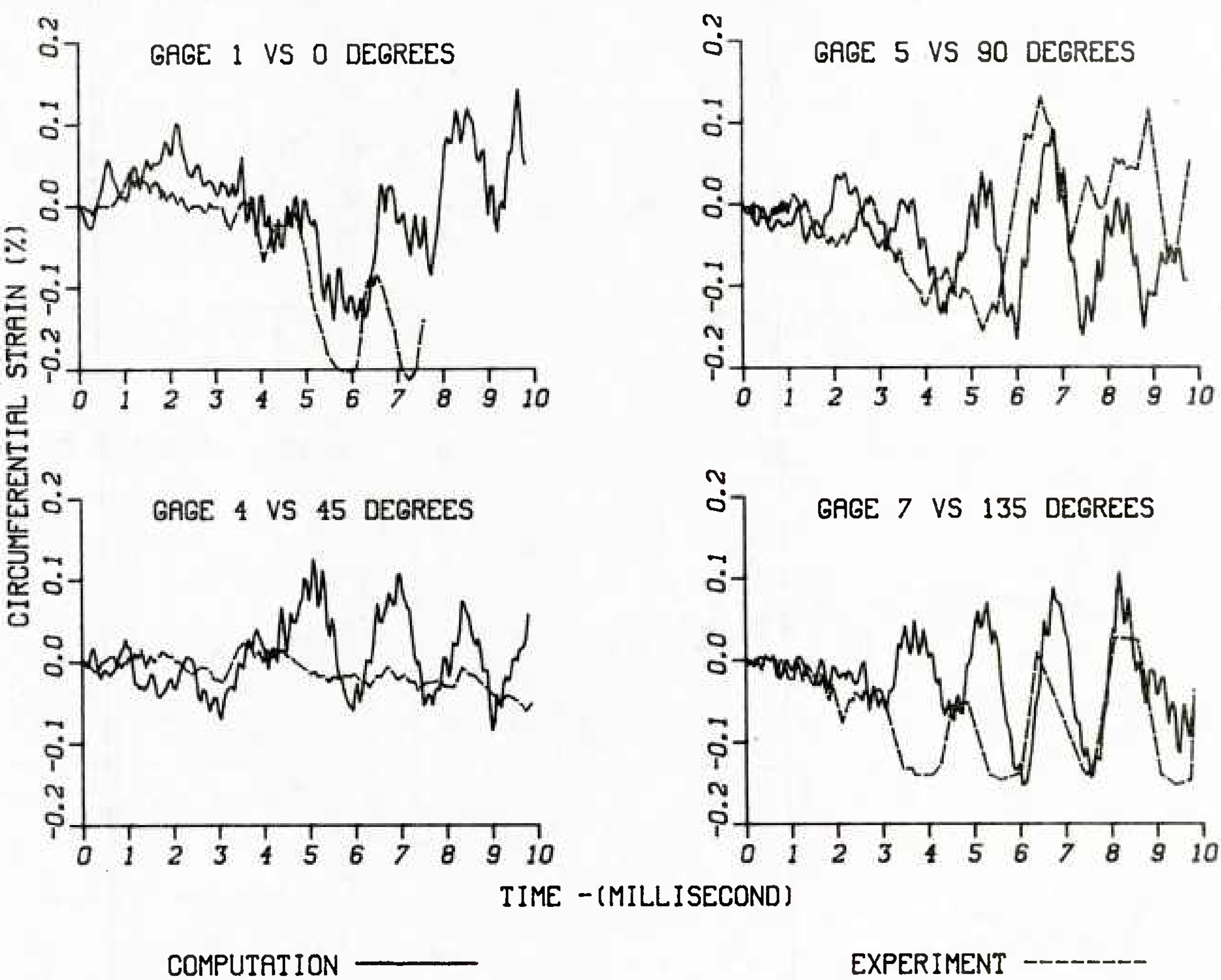

Figure 12. Comparison of circumferential strain histories recorded at mid-cylinder gage locations and computed by the nonlinear analysis at corresponding stations.

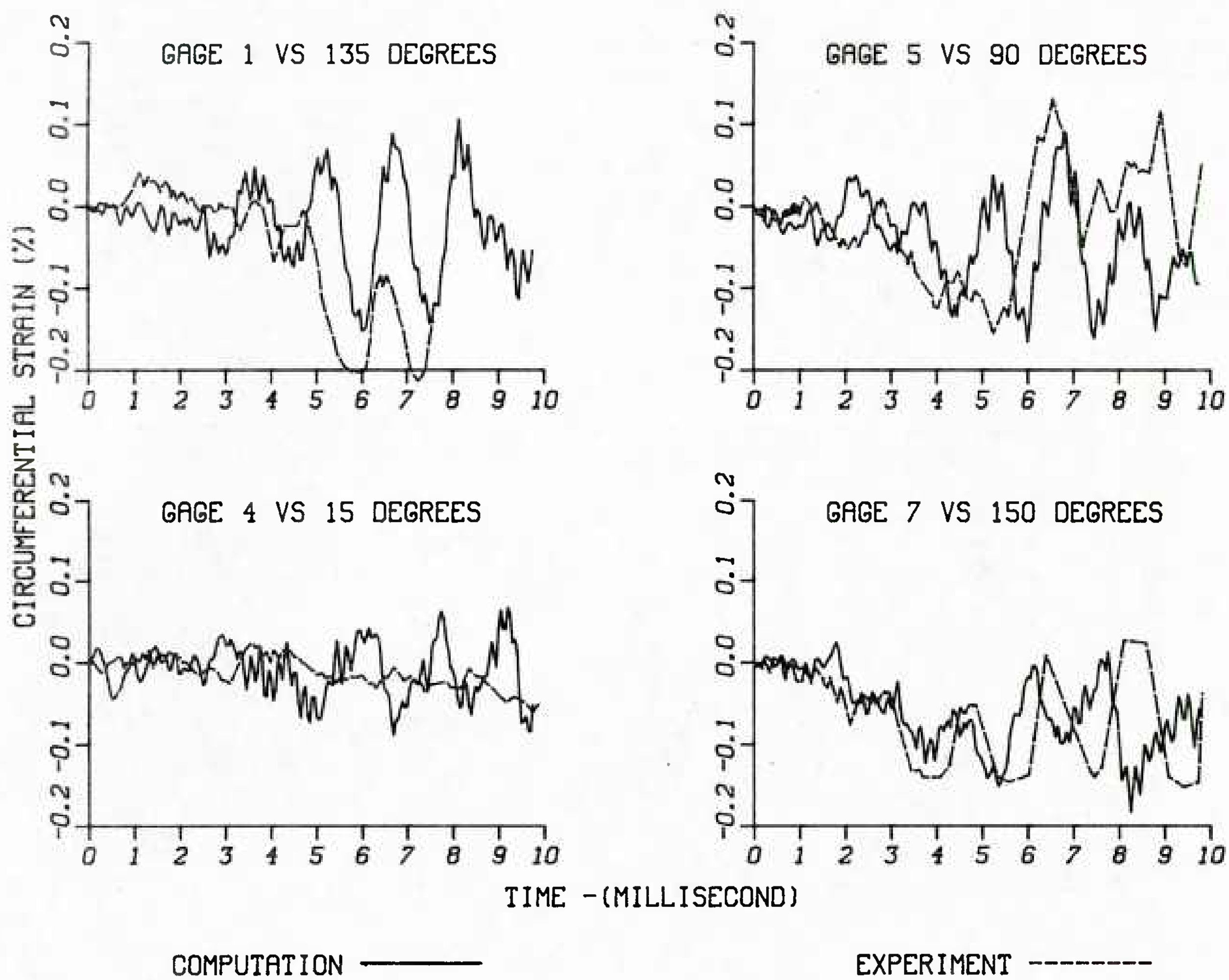

Figure 13. Comparison of circumferential strain histories recorded at mid-cylinder gage locations and computed by the nonlinear analysis at circumferential stations selected for optimum correlation.

- Uncertainties and lack of uniformity in the material properties of the experimental cylinder, especially the plastic yield stress (recall the welded seam and some yielding caused by using strap clamps at the ends).

- The vibratory modes excited by the nonuniform loading eventually combining to produce a deformation that exceeded the yield strain at some points.

- Uncertainty about the pressure loading distribution during the first 10 milliseconds (recall the assumption of axial uniformity).

- Changes in the intensity and distribution of the pressure loading after the first 10 milliseconds.

Of these possibilities, it is most unlikely that geometric imperfections or local weaknesses in the material caused plastic deformation, since their effects would have been manifested soon after buckling occurred during the first 10 milliseconds. More likely, but not too probable for the same reason, is the possibility that the vibratory modes eventually combined to produce plasticity. The assumption of axial uniformity of the pressure distribution is probably quite good for the first 10 milliseconds, giving a fairly close simulation of loading imposed on the cylinder, since not enough time had elapsed for reflections from the test fixture and the ends of the shock tube to distort the flow in the test section. Hence, the likeliest reason for the permanent plastic deformation is the changes that the pressure loading undergoes during late-times. More specifically, as the air emptied out of the shock tube, rarefaction waves proceeding from the open end probably accelerated the flow velocity sufficiently to distort the distribution of the drag loads on the cylinder and locally magnify the pressure level, resulting in the further (plastic) deformation of the cylinder. Moreover, the resulting late-time pressure distribution would probably have been axially nonuniform, making the gage readings, had they been recorded at all, unrepresentative of the loading on the cylinder. For this reason, the lack of late-time loading data, and the extensive computational effort that it would have involved, no attempt was made to carry the calculations past the initial 10 milliseconds.

Whatever the cause of the plastic deformation, it is significant that both the von Mises buckling analysis and the ADINA nonlinear solution predict a buckling pattern very similar to that measured on the cylinder. Moreover, since it is likely that plastic yielding would occur where the strains are extreme (i.e., where the curvature is greatest) and since the computed buckling pattern, although elastic, does not change much with time (see Fig. 10), it is reasonable to expect that the same pattern would persist into the late-time plastic flow phase, justifying to a certain degree the comparison of the post test shape and the computed elastic cross-sections.

XI. SUMMARY AND CONCLUSIONS

The subspace iteration technique in the ADINA code was found to effectively calculate the frequencies and mode shapes of the test cylinder. The first 20 modes were calculated using the ADINA 16-noded shell element and the first 6 modes using the ADINA 3-noded triangular plate element. Frequencies and mode shapes predicted by both elements were found to correlate excellently with each other and with those from a Rayleigh-Ritz analysis based on the Donnell shell equations.

Good overall correlation with the data from the shock tube cylinder test was obtained using the ADINA 16-noded curved shell element. The strain histories calculated from the linear solution corresponded fairly well with the strains recorded for the axially oriented gages over the entire interval. The correspondence with the strains for the circumferentially oriented gages was also good, but only for the first 4 milliseconds, after which the strains at some gage locations show an increasing divergence. The subsequent geometric nonlinear analysis showed dynamic buckling to be the principal cause of this divergence. The strain histories computed by the nonlinear analysis showed the same significant increase in the circumferential components occurring after 4 milliseconds. Although the circumferential strain gage data did not completely agree with the computed stain histories at the corresponding gage locations, other locations were found at which agreement was considerably improved.

The deflection pattern predicted by the nonlinear analysis and the post-test deflection measurements were found to agree substantially in the number of buckling waves and the magnitude of the deformation. That the buckling pattern on the cylinder did not coincide exactly with that measured on the test specimen was most probably due to geometric and material imperfections and the sensitivity of buckling phenomena to such defects. However, given the difficulty of making accurate buckling predictions due to uncertainties in material properties, specimen geometry, and loads definition, and that perhaps a less crude finite element mesh should have been used, the finite element analysis succeeded in generally reproducing the salient features of measured deformation to a remarkable degree.

This investigation conclusively demonstrated that dynamic buckling had a significant effect on the blast response of the cylinder and that the ability of the finite element calculations to accurately predict the deflections hinged on correctly modeling this phenomenon. The calculations also emphasized the importance of choosing an appropriate finite element modeling to perform the transient analysis of shell-like structures, in particular, whenever there is a reasonable likelihood of dynamic buckling occurring.

ACKNOWLEDGMENTS

We wish to acknowledge Mr. Richard J. Pearson of the BRL for providing the test data and for his helpful advice, the NBC Protection Research and Development Institute of the Federal Republic of Germany for enabling the second author to participate in the investigation under the auspices of the US/GE Scientist and Engineer Exchange Program, and the Nuclear Weapon Effects Project Office of the US Army Harry Diamond Laboratory for funding the investigation.

REFERENCES

1. *ADINA, A Finite Element Program for Automatic Dynamic Incremental Nonlinear Analysis, Users Manual,* Report AE 84-1, ADINA Engineering Inc., Watertown, MA, December 1984.

2. Pearson, R. J., Wisniewski, H. L., Szabados, P. D., and Wilson, A. W., *The Effects of Thermal/Blast Synergism on the Nuclear Vulnerability of a Generic Aircraft Structure,* Technical Report ARBRL-TR-02540, US Army Ballistic Research Laboratory, Aberdeen Proving Ground, MD, January 1984.

3. Gregory, F. H. and Pearson, R. J., "Analytical and Experimental Studies of the Response of a Cylinder to Nuclear Thermal/Blast Loads," *Proceeding of the 1982 Army Science Conference,* West Point, NY, June 1982.

4. Bertrand, B. P., *BRL Dual Shock Tube Facility,* Memorandum Report MR-2001, US Army Ballistic Research Laboratory, Aberdeen Proving Ground, MD, August 1969.

5. Bathe, K.-J., and Bolourchi, S., "A Geometric and Material Nonlinear Plate and Shell Element," *Journal of Computers and Structures,* Vol. 11, pp. 23-48, 1980.

6. Kraus, H., *Thin Elastic Shells,* John Wiley & Sons, New York, 1973, pp. 297-302.

7. Bathe, K.-J., and Ho, L. W., "A Simple and Effective Element for Analysis of General Shell Structures," *Journal of Computers and Structures,* Vol. 13, 1981, pp. 673-681.

8. Santiago, J. M., Klaus, M. H., and Wisniewski, H. L., *Finite Element Frequency Analysis of a Thin-Walled Cylinder,* to be published as report by US Army Ballistic Research Laboratory, Aberdeen Proving Ground, MD.

9. Timoshenko, S., and Goodier, J. N., *The Theory of Elasticity,* McGraw-Hill, New York, 1951, pp. 18, eq. (c).

10. Strang, G., and Fix, G. J., *Analysis of the Finite Element Method,* Prentice-Hall, Englewood Cliffs, NJ, 1973, pp. 228-236.

11. Timoshenko, S., *Theory of Elastic Stability,* McGraw-Hill, New York, 1936, pp. 450, eq. (270).

12. Lindberg, H. E., and Florence, A. L., *Dynamic Pulse Buckling - Theory and Experiment,* Report Number DNA 6503H, Defense Nuclear Agency, Washington, DC, 1 February 1983 pp. 1-3, 158-201.

APPENDIX: CYLINDER SURFACE DEFLECTIONS

The following pages of this appendix contain computer plots of the deformed surface of the cylinder at select times. They were calculated by the ADINA program using the total Lagrangian method for modeling geometric nonlinear effects. The material was assumed to be linearly elastic. For the real times indicated, each page shows a longitudinal cross-section through the crown line, a lateral cross-section through the mid-cylinder, and an isometric of the surface deflection. The deflections are shown magnified by a factor of ten (10) relative to the cylinder dimensions. The plots trace the development of dynamic buckling beginning at 3.5 millisecond. The deflections do not become larger because no plastic yielding occurs and hence no permanent deformation can result.

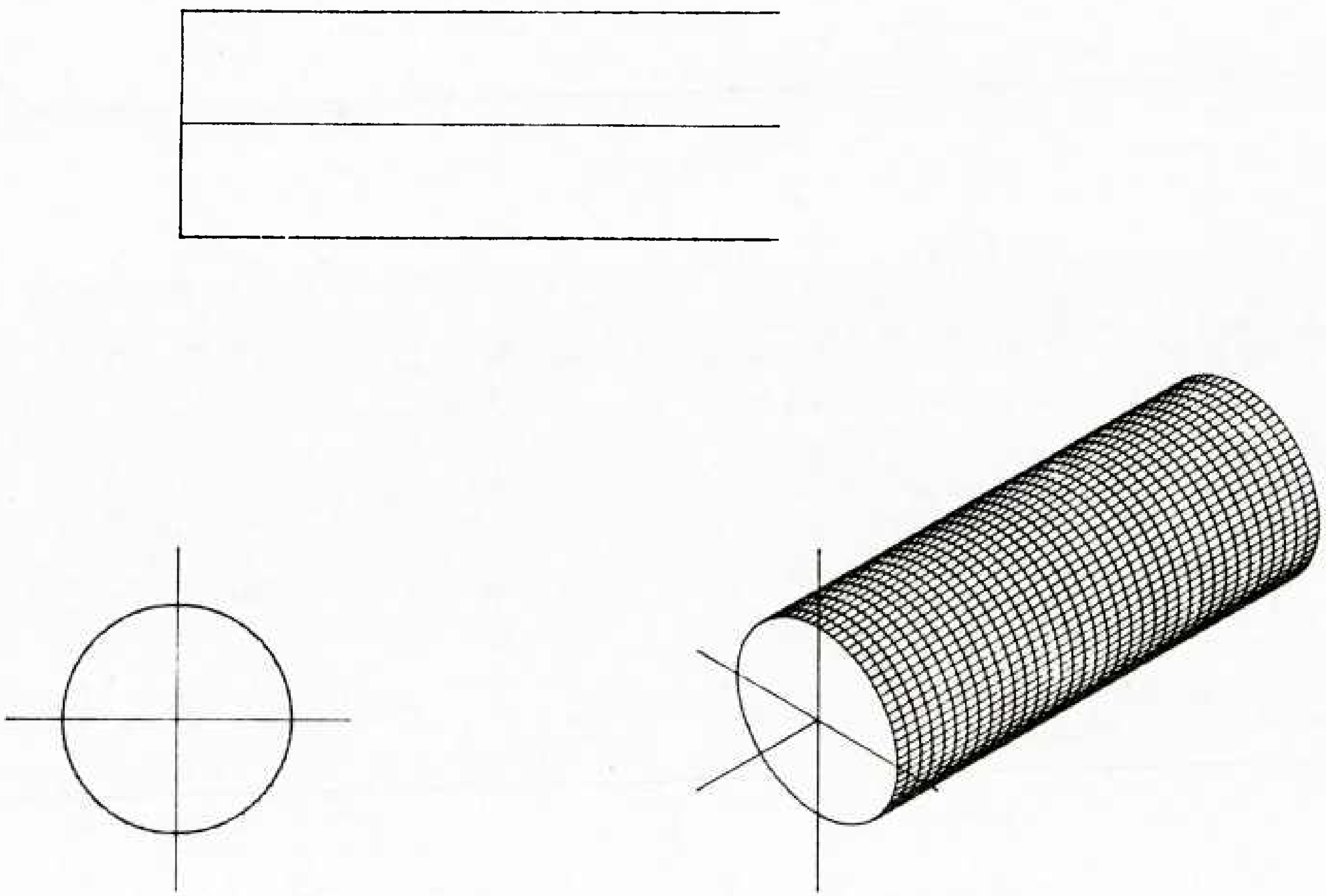

CYCLE 0
0.000MICROSECONDS

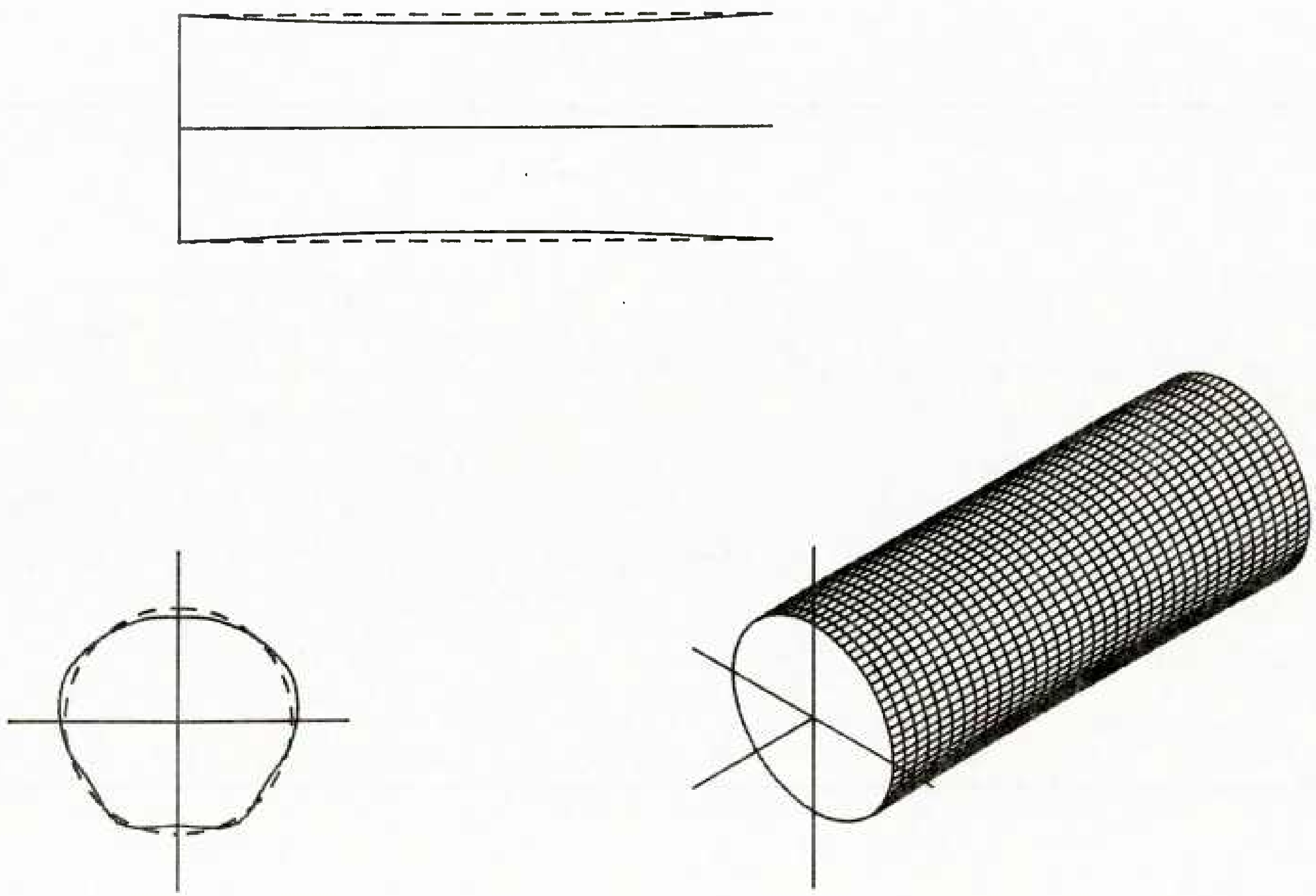

CYCLE 70
3500.000MICROSECONDS

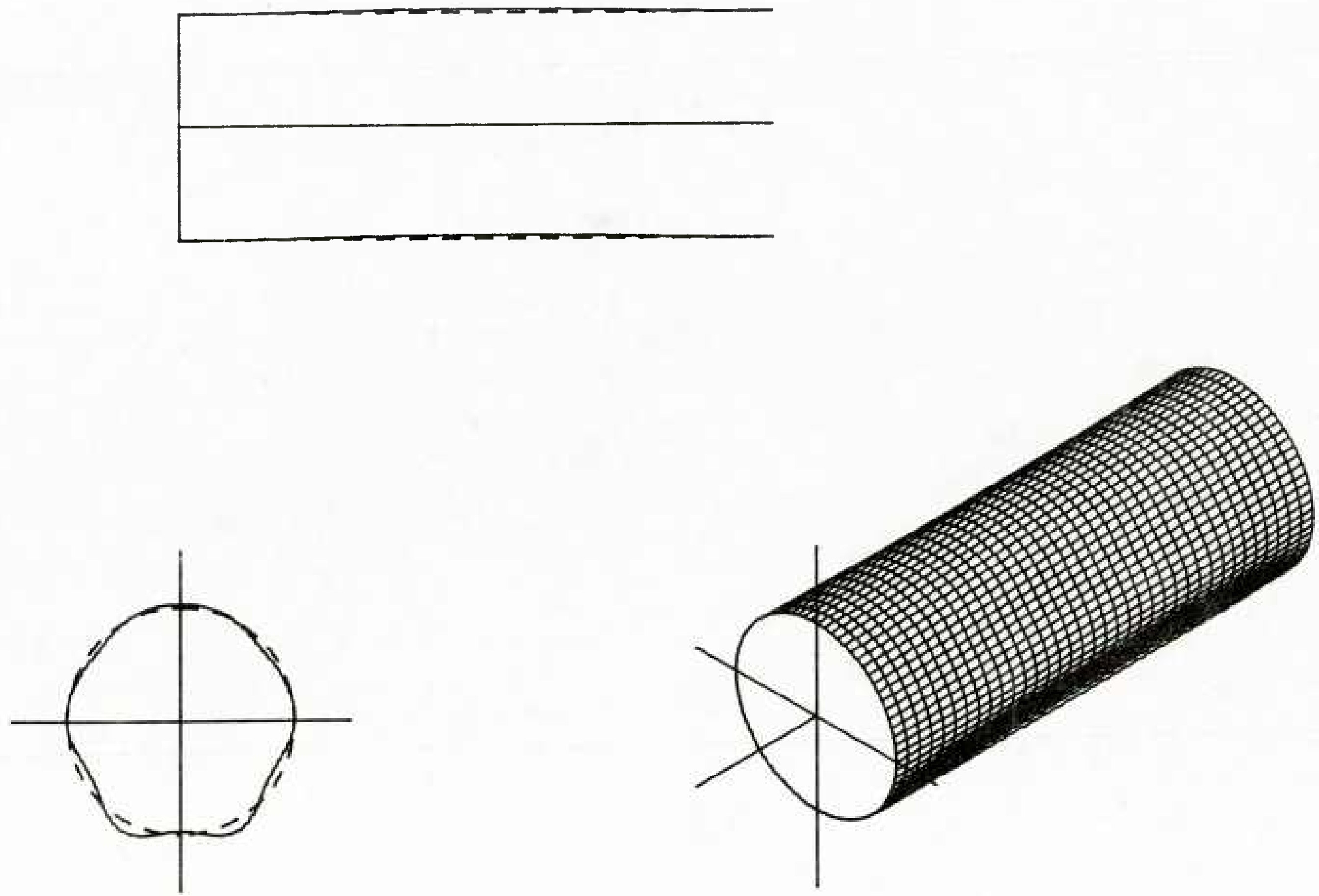

CYCLE 80
4000.000MICROSECONDS

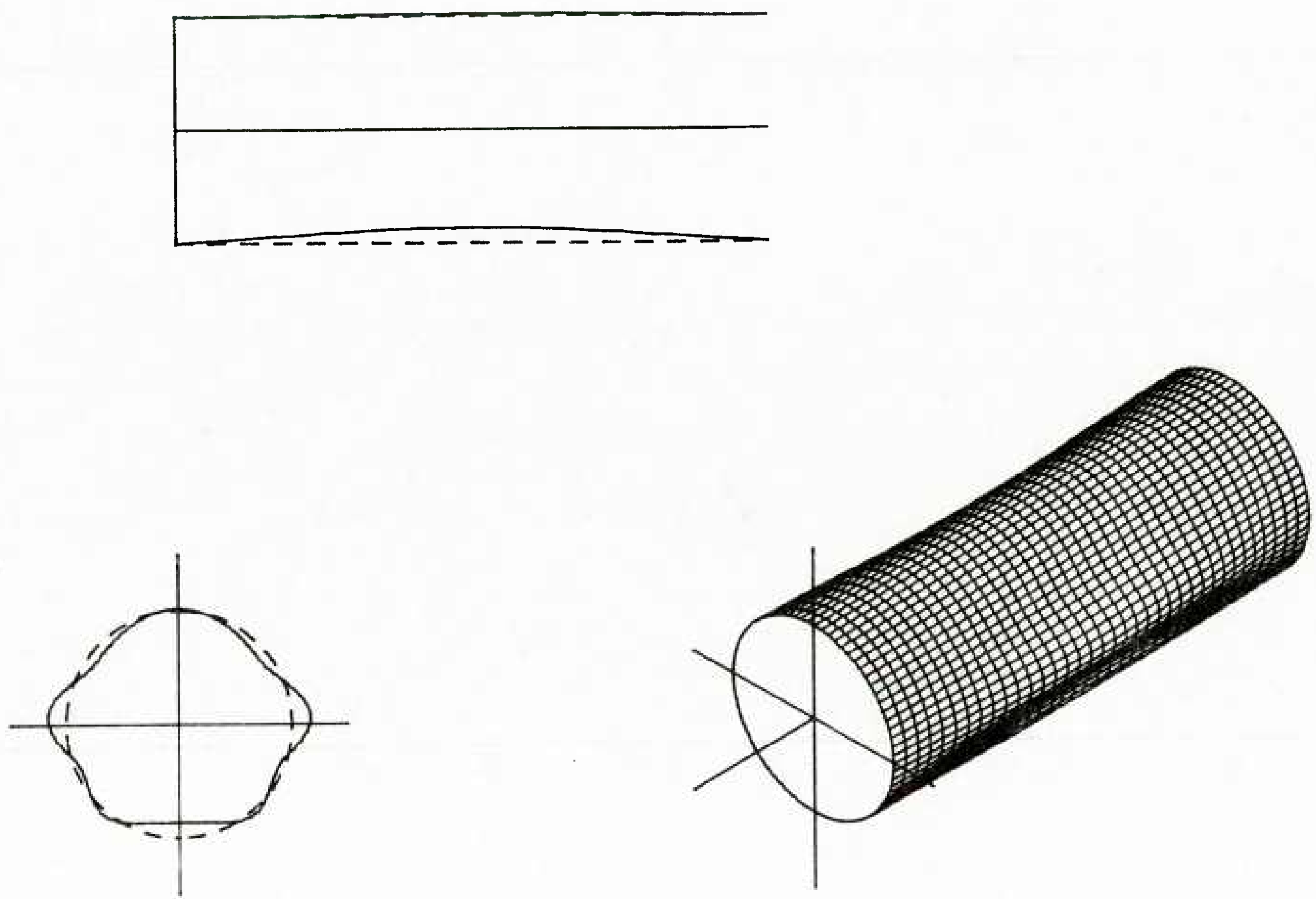

CYCLE 90
4500.000MICROSECONDS

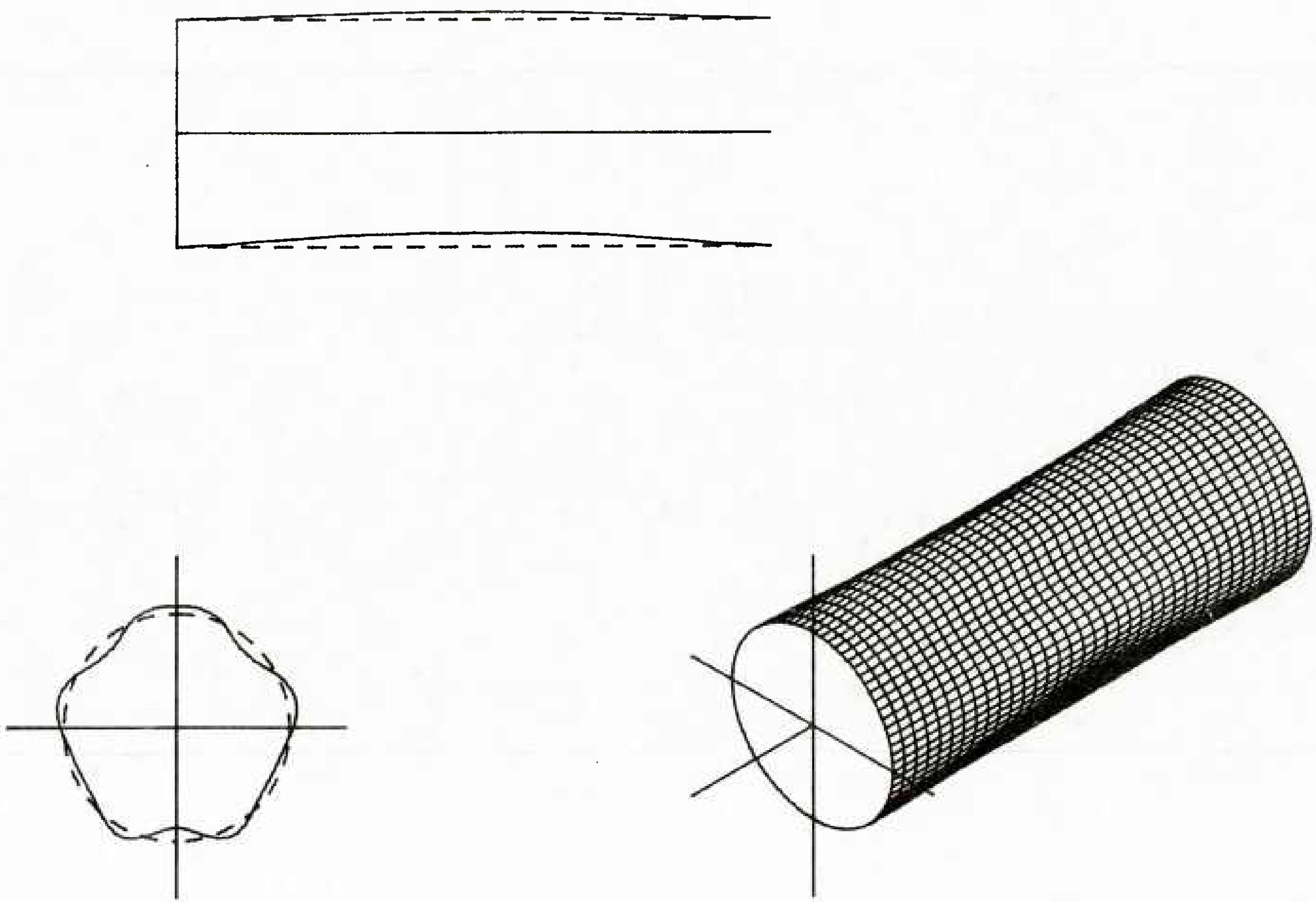

CYCLE 100
5000.000MICROSECONDS

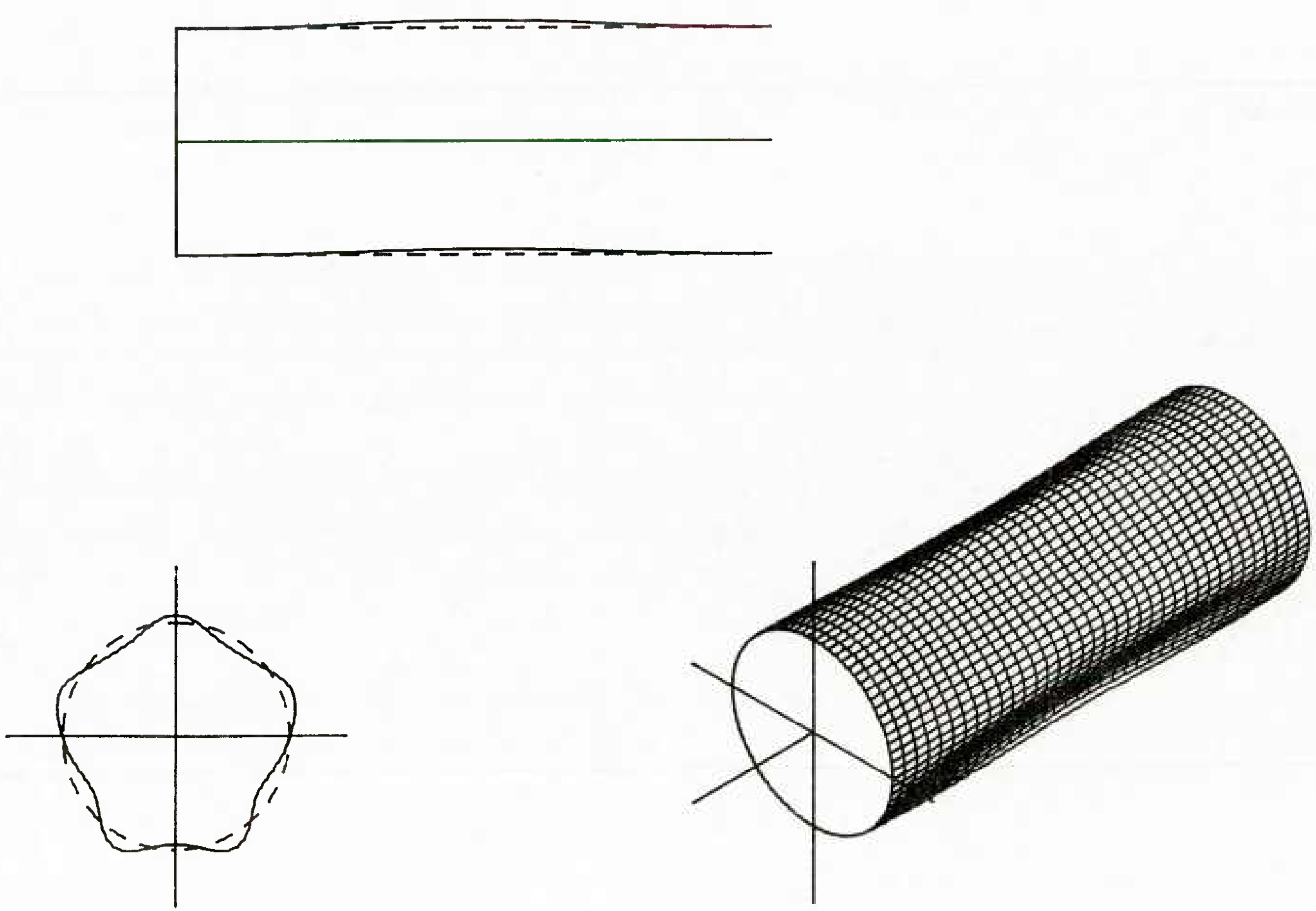

CYCLE 110
5500.000MICROSECONDS

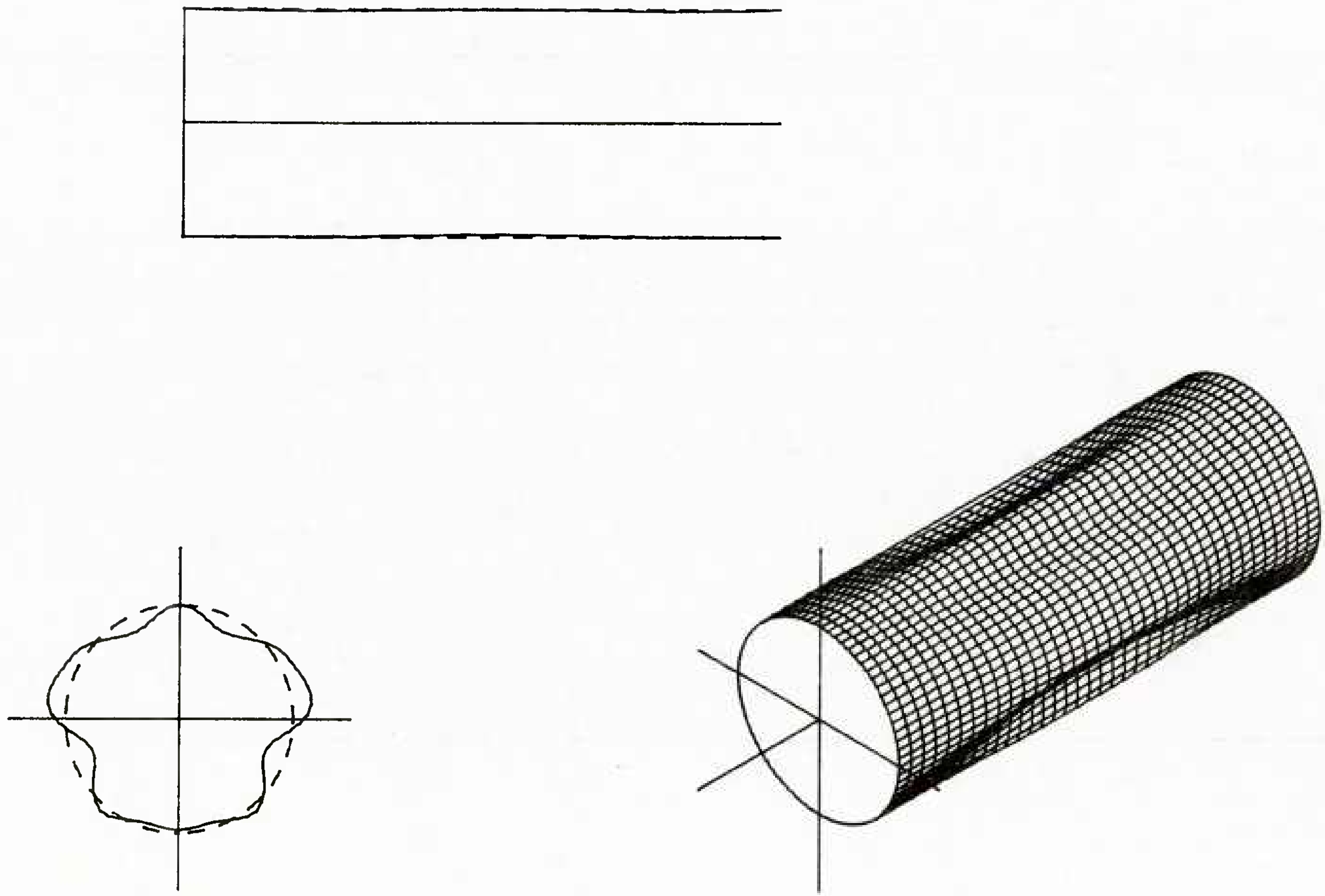

CYCLE 120
6000.000MICROSECONDS

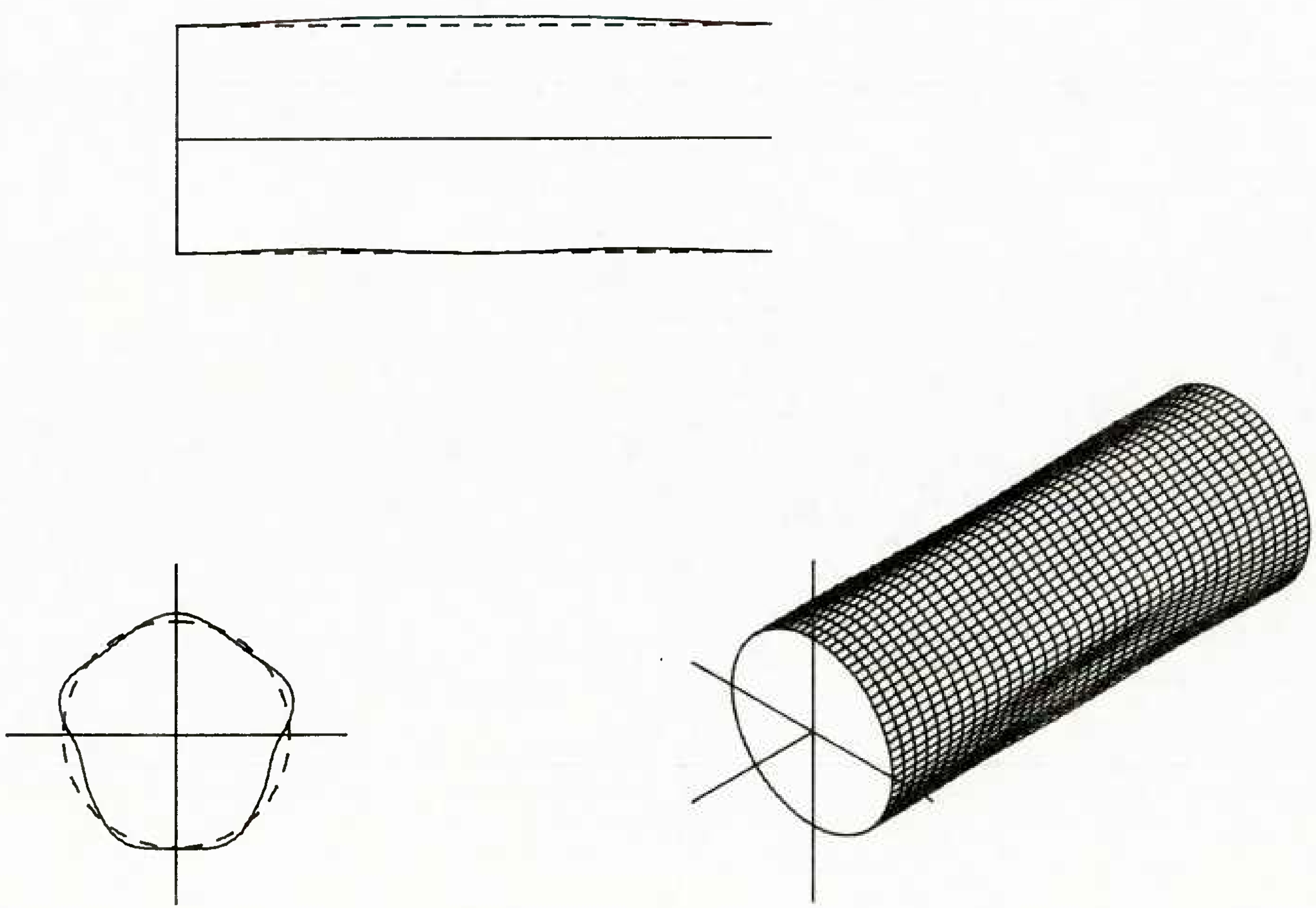

CYCLE 130
6500.000MICROSECONDS

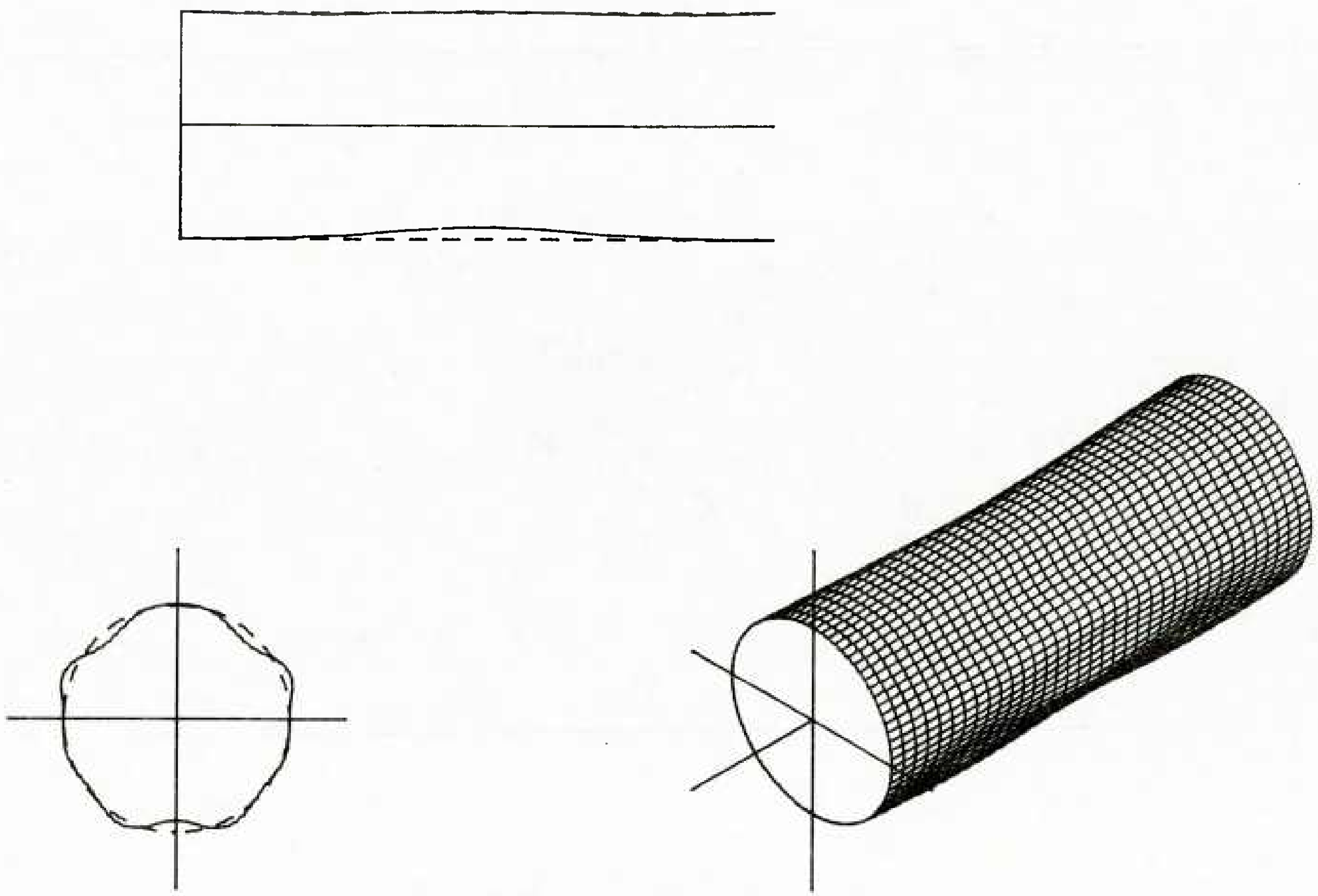

CYCLE 140
7000.000MICROSECONDS

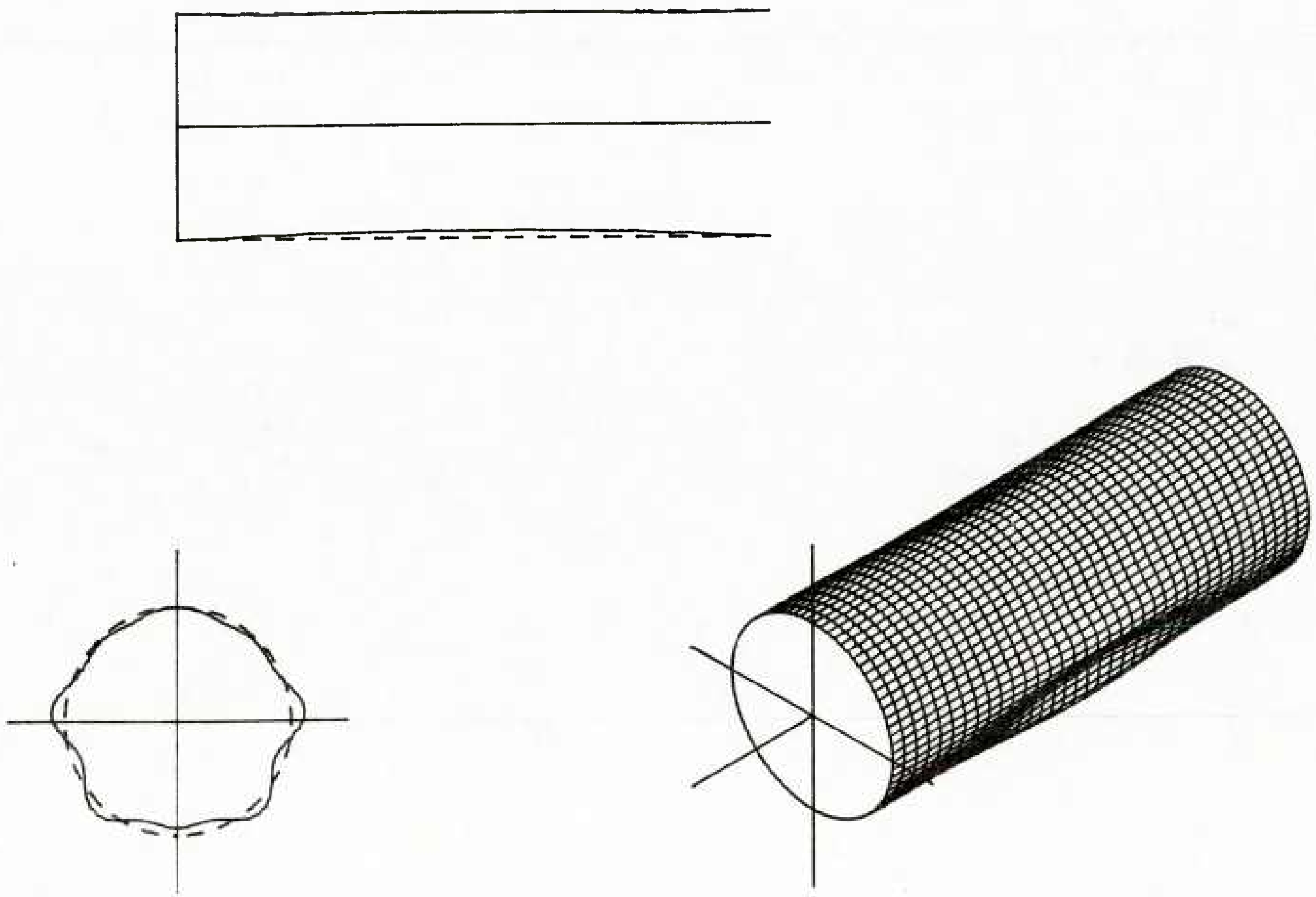

CYCLE 150
7500.000MICROSECONDS

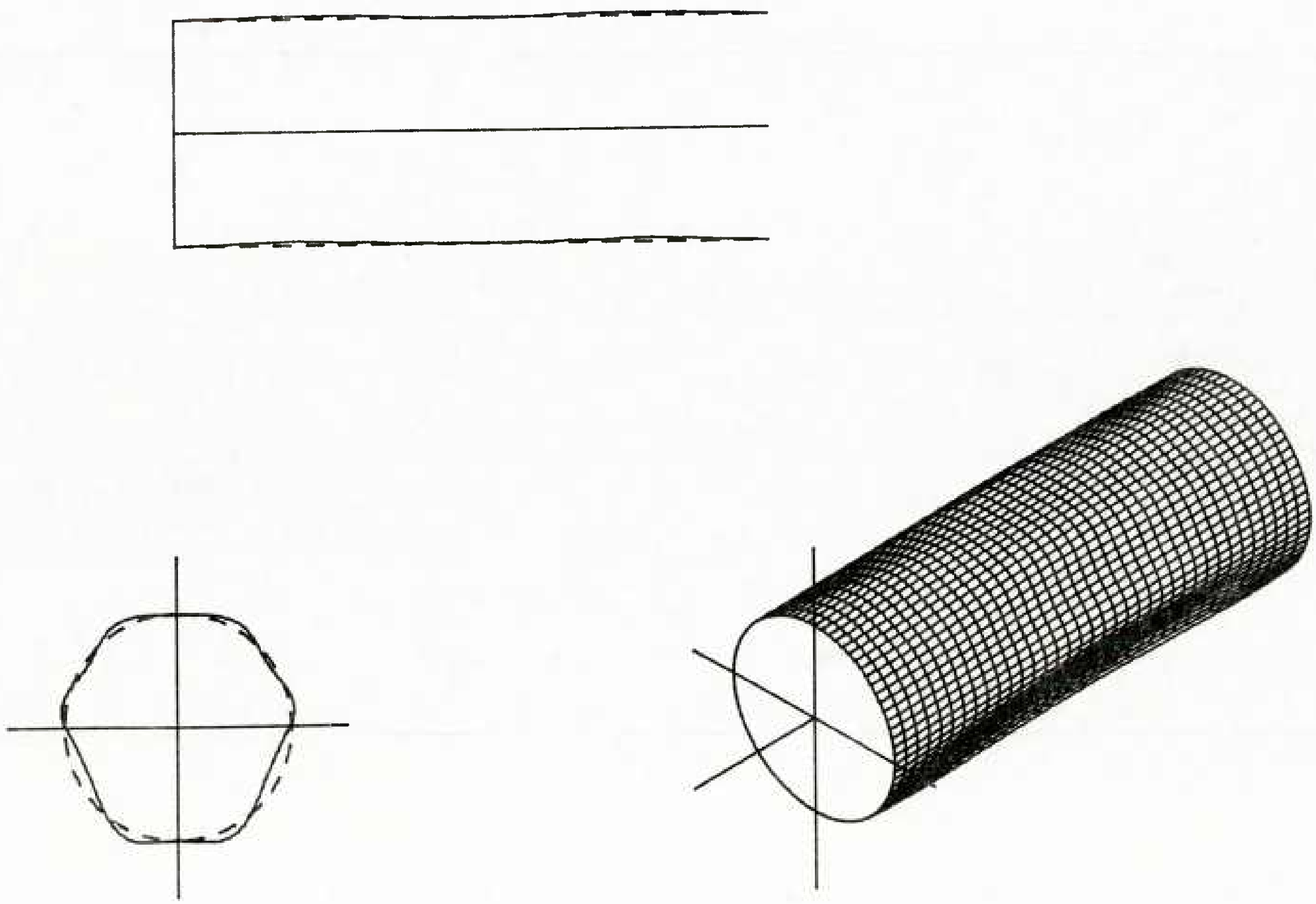

CYCLE 160
8000.000MICROSECONDS

DISTRIBUTION LIST

No. of Copies	Organization
12	Administrator Defense Technical Information Center ATTN: DTIC-FDAC Cameron Station, Bldg 5 Alexandria, VA 22304-6145
1	Director of Defense Research & Engineering ATTN: DD/TWP Washington, DC 20301
1	Asst. to the Secretary of Defense (Atomic Energy) ATTN: Document Control Washington, DC 20301
4	Director Defense Advanced Research Projects Agency ATTN: Tech Lib Dr. E. Van Reuth Dr. G. Farnum Dr. B. Wilcox 1400 Wilson Boulevard Arlington, VA 22209
1	Deputy Assistant Secretary of the Army (R&D) Department of the Army Washington, DC 20310
9	Director Defense Nuclear Agency ATTN: DDST TIPL, Tech Lib SPSS, K. Goering SPTD, T. Kennedy SPAS, P.R. Rohr G. Ullrich STSP, COL Kovel NATD NATA Washington, DC 20305

No. of Copies	Organization
2	Commander Field Command, DNA ATTN: FCPR FCTMOF Kirtland AFB, NM 87117
1	Commander Field Command, DNA Livermore Branch ATTN: FCPRL P.O. Box 808 Livermore, CA 94550
1	HQDA DAMA-ART-M Washington, DC 20310
10	C.I.A. OIR/DB/Standard GE47 HQ Washington, DC 20505
1	Program Manager US Army BMD Program Office ATTN: John Shea 5001 Eisenhower Avenue Alexandria, VA 22333
2	Director US Army BMD Advanced Technology Center ATTN: CRDABH-X CRDABH-S Huntsville, AL 35807
1	Commander US Army BMD Command ATTN: BDMSC-TFN, N.J. Hurst P.O. Box 1500 Huntsville, AL 35807
1	Commander US Army Engineer Division ATTN: HNDED-FD P.O. Box 1500 Huntsville, AL 35807

DISTRIBUTION LIST

No. of Copies	Organization
2	Deputy Chief of Staff for Operations and Plans ATTN: Technical Library Director of Chemical & Nuclear Operations Department of the Army Washington, DC 20310
3	Commander US Army Engineers Waterways Experiment Station ATTN: Technical Library Jim Watt Jim Ingram P.O. Box 631 Vicksburg, MS 39180
1	Commander US Army Materiel Command ATTN: AMCDRA-ST 5001 Eisenhower Avenue Alexandria, VA 22333-0001
3	Commander US Army Armament RD&E Center ATTN: SMCAR-TDC SMCAR-MSI SMCAR-TE, W. H. Moore, III W. Reiner Dover, NJ 07801-5001
1	Commander US Army Armament, Munitions and Chemical Command ATTN: AMSMC-IMP-L Rock Island, IL 61299-7300
1	Commander US AMCCOM ARDEC CCAC Benet Weapons Laboratory Armament R&D Center ATTN: SMCAR-CCB-TL Watervliet, NY 12189-4050

No. of Copies	Organization
1	Commander US Army Aviation Research and Development Command ATTN: AMSAV-ES 4300 Goodfellow Boulevard St. Louis, MO 63120-1798
1	Director US Army Aviation Research and Technology Activity Ames Research Center Moffett Field, CA 94035-1099
1	Commander U.S. Army Communications - Electronics Command (CECOM) CECOM R&D Technical Library ATTN: AMSEL-IM-L, B 2700 Fort Monmouth, NJ 07703-5000
11	Director US Army Harry Diamond Labs ATTN: DELHD-TA-L DRXDO-TI/002 DRXDO-NP DELHD-RBA, J. Rosado Mr. James Gaul Mr. L. Belliveau Mr. J. Meszaros Mr. J. Gwaltney Mr. Bill Vault Mr. R. J. Bostak Dr. W. J. Schuman, Jr. 2800 Powder Mill Road Adelphi, MD 20783
1	Commander US Army Missile Command ATTN: AMSMI-RD-DE-UB, H. Greene Redstone Arsenal, AL 35898-5249
1	Director US Army Missile and Space Intelligence Center ATTN: AIAMS-YDL Redstone Arsenal, AL 35898-5500

DISTRIBUTION LIST

No. of Copies	Organization
2	Commander US Army Natick Research and Development Center ATTN: DRXRE, Dr. D. Sieling STRNC-UE, J. Calligeros Natick, MA 01762
2	Commander US Army Tank Automotive Research and Development Command ATTN: AMSTA-TSL DRDTA-ZSS, J. Thompson Warren, MI 48397-5000
1	Commander US Army Foreign Science and Technology Center ATTN: Rsch & Cncepts Br 220 7th Street , NE Charlottesville, VA 22901
4	Commander US Army Materials Technology Laboratory ATTN: Technical Library SLCMT-T, J. Mescall SLCMT-T, R. Shea SLCMT-T, S. C. Chou Watertown, MA 02172-0001
5	Commander US Army Research Office ATTN: Dr. J. Chandra Dr. G. L. Anderson Dr. G. Meyer Dr. E. Saibel P.O. Box 12211 Research Triangle Park, NC 27709
1	Commander US Army TRADOC ATTN: DCST&E Fort Monroe, VA 23651
1	Director US Army TRADOC Analysis Center ATTN: ATOR-TSL White Sands Missile Range NM 88002-5502
2	Commandant US Army Infantry School ATTN: ATSH-CD-CS-OR Fort Benning, GA 31905-5400
1	Commander US Army War College ATTN: Lib Carlisle Barracks, PA 17013
1	Commander US Army Command and General Staff College ATTN: Archives Fort Leavenworth, KS 66027
1	Commander U.S. Army Development and Employment Agency ATTN: MODE-ORO Fort Lewis, WA 98433-5000
1	Commandant Interservice Nuclear Weapons School ATTN: Technical Library Kirtland AFB, NM 87115
1	Chief of Naval Research ATTN: N. Perrone Department of the Navy Arlington, VA 22217
1	Office of Naval Research ATTN: Dr. Faulstich, Code 23 800 N. Quincy Street Arlington, VA 22217
1	Director Strategic Systems Projects Ofc ATTN: NSP-43, Tech Library Department of the Navy Washington, DC 20360
1	Commander Naval Facilities Engineering Command Washington, DC 20360

DISTRIBUTION LIST

No. of Copies	Organization
3	Officer-in-Charge(Code L31) Naval Constr Btn Center Civil Engineering Laboratory ATTN: Stan Takahashi R. J. Odello Technical Library Port Hueneme, CA 93041
1	Commander David W. Taylor Naval Ship R & D Ctr ATTN: Lib Div, Code 522 Bethesda, MD 20084-5000
1	Commander Naval Surface Weapons Center ATTN: DX-21, Library Br. Dahlgren, VA 22448-5000
2	Commander Naval Surface Weapons Center ATTN: Code WA501, Navy Nuclear Programs Office Code WX21, Tech Library Silver Spring, MD 20902-5000
1	Commander Naval Weapons Center ATTN: Code 533, Tech Lib China Lake, CA 93555-6001
2	Commander Naval Research Laboratory ATTN: Code 2027, Tech Lib Code 6382, Dr. Peter Matic Washington, DC 20375
1	Superintendent Naval Postgraduate School ATTN: Code 2124, Technical Reports Library Monterey, CA 93940
1	AFWL/SUL Kirtland AFB, NM 87117-6008

No. of Copies	Organization
1	Air Force Armament Laboratory ATTN: AFATL/DOIL (Tech Info Center) Eglin AFB, FL 32542-5438
1	AFESC/RDCS ATTN: Paul Rosengren Tyndall AFB, FL 32403
1	AFWL/NTES, R. Henny Kirtland AFB, NM 87117-6008
1	AFWL/NTED, J. W. Aubrey Kirtland AFB, NM 87117-6008
2	Director Lawrence Livermore Lab. ATTN: Tech Info Dept L-3 Dr. M. L. Wilkins P.O. Box 808 Livermore, CA 94550
3	Director Los Alamos National Laboratory ATTN: Doc Control for Rpts Lib FC-2/FCDNA, WP/DNA MS F635 P.O. Box 1663 Los Alamos, NM 87545
3	Director Sandia National Laboratories ATTN: Doc Control for 3141 Sandia Rpt Collection L. J. Vortman P.O. Box 5800 Albuquerque, NM 87185
2	Director Sandia National Laboratories Livermore Laboratory ATTN: Doc Control for Tech Lib Dr. D. Bamman P.O. Box 969 Livermore, CA 94550

DISTRIBUTION LIST

No. of Copies	Organization
1	Director National Aeronautics and Space Administration Scientific & Tech Info Fac P.O. Box 8757 Baltimore-Washington International Airport, MD 21240
1	Director NASA-Ames Research Center Applied Computational Aerodynamics Branch ATTN: MS 202-14, Dr. T. Holtz Moffett Field, CA 94035
1	Director Jet Propulsion Laboratory ATTN: Lib (TDS) 4800 Oak Grove Drive Pasadena, CA 91103
1	National Bureau of Standards ATTN: Dr. Timothy Burns, Rm A151 Technology Building Gaithersburg, MD 20899
1	Battelle Memorial Institute ATTN: Technical Library Dr. A. B. Chaudhary 505 King Avenue Columbus, OH 43201
1	Director Battelle Advanced Concepts Lab. Columbus Division ATTN: Dr. R. Stein Warren, MI 48090
3	Aberdeen Research Center ATTN: N.H. Ethridge J. Keefer Library P.O. Box 548 30 Diamond Street Aberdeen, MD 21001

No. of Copies	Organization
1	Adina R&D, Inc. ATTN: Dr. M. Kojic 71 Elton Avenue Watertown, MA 02172
1	Aerospace Corporation ATTN: Tech Info Services P.O. Box 92957 Los Angeles, CA 90009
1	Agbabian Associates ATTN: M. Agbabian 250 North Nash Street El Segundo, CA 90245
1	The BDM Corporation ATTN: Richard Hensley P.O. Box 9274 Albuquerque International Albuquerque, NM 87119
1	Black & Veach Consulting Engineers ATTN: H. D. Laverentz 1500 Meadow Lake Parkway Kansas City, MO 64114
1	The Boeing Company ATTN: Aerospace Library P.O. Box 3707 Seattle, WA 98124
1	California Research & Technology, Inc. ATTN: F. Sauer Suite B 130 11875 Dublin Blvd Dublin, CA 94568
1	California Research & Technology, Inc. ATTN: M. Rosenblatt 20943 Devonshire Street Chatsworth, CA 91311

DISTRIBUTION LIST

No. of Copies	Organization
1	Carpenter Research Corporation ATTN: H. Jerry Carpenter Suite 424 904 Silver Spur Road Rolling Hills Estates, CA 90274
1	Dynamics Technology, Inc. ATTN: D. T. Hove Suite 300 21311 Hawthorne Blvd. Torrance, CA 90503
1	Forestall Research Center Aeronautical Engineering Lab Princeton University ATTN: Dr. A. Eringen 600 Second Street, NE Princeton, NJ 08540
1	Goodyear Aerospace Corporation ATTN: R. M. Brown, Bldg 1 Shelter Engineering Litchfield Park, AZ 85340
1	Honeywell, Inc. Defense Systems Division ATTN: Dr. Gordon Johnson 600 Second Street, NE Hopkins, MN 55343
6	Kaman AviDyne ATTN: Dr. R. Reutenick (4 cys) Mr. S. Criscione Mr. R. Milligan 83 Second Avenue Northwest Industrial Park Burlington, MA 01830
3	Kaman Sciences Corporation ATTN: Library P. A. Ellis F. H. Shelton 1500 Garden of the Gods Road Colorado Springs, CO 80907
1	Kaman-TEMPO ATTN: DASIAC P.O. Drawer QQ 816 State Street Santa Barbara, CA 93102
1	Kaman-TEMPO ATTN: E. Bryant, Suite UL-1 715 Shamrock Road Bel Air, MD 21014
1	Lockheed Missiles & Space Co. ATTN: J. J. Murphy, Dept. 81-11, Bldg. 154 P.O. Box 504 Sunnyvale, CA 94086
1	Martin-Marietta Aerospace Orlando Division ATTN: G. Fotieo P.O. Box 5837 Orlando, FL 32805
1	Martin-Marietta Aerospace ATTN: M.P. 17, Dr. Clayton McKindray 103 Cheasepeake Park Plaza, MD 21220
2	McDonnell Douglas Astronautics Corporation ATTN: Robert W. Halprin K.A. Heinly 5301 Bolsa Avenue Huntington Beach, CA 92647
1	New Mexico Engineering Research Institute (CERF) ATTN: J. Leigh P.O. Box 25 UNM Albuquerque, NM 87131
2	Physics International Corporation 2700 Merced Street San Leandro, CA 94577

DISTRIBUTION LIST

No. of Copies	Organization
2	R&D Associates ATTN: Technical Library Allan Kuhl P.O. Box 9695 Marina del Rey, CA 90291
1	R&D Associates ATTN: Gary P. Ganong P.O. Box 9335 Albuquerque, NM 87119
2	Science Applications, Inc. ATTN: W. Layson John Cockayne PO BOX 1303 1710 Goodridge Drive McLean, VA 22102
1	Science Applications, Inc. ATTN: Technical Library 1250 Prospect Plaza La Jolla, CA 92037
2	Southwest Research Institute ATTN: A. B. Wenzel Dr. U. Lindholm 8500 Culebra Road San Antonio, TX 78228
7	SRI International ATTN: Dr. G. R. Abrahamson Dr. Donald R. Curran Dr. Donald A. Shockey Dr. Lynn Seaman Dr. D. Erlich Dr. A. Florence Dr. R. Caligiuri 333 Ravenswood Avenue Menlo Park, CA 94025
2	Systems, Science and Software ATTN: C. E. Needham Lynn Kennedy PO Box 8243 Albuquerque, NM 87198

No. of Copies	Organization
3	Systems, Science and Software ATTN: Technical Library R. Duff K. Pyatt PO Box 1620 La Jolla, CA 92037
1	Texas Instrument ATTN: MS 10-13, Dr. W. D. Rolph III Attleboro, MA 02703
1	TRW - Ballistic Missile Division ATTN: H. Korman, Mail Station 526/614 P.O. Box 1310 San Bernadino, CA 92402
2	TRW Systems Group ATTN: Benjamin Sussholtz Stanton Fink One Space Park Redondo Beach, CA 90278
1	Wilfred Baker Engineering ATTN: Dr. Wilfred E. Baker P.O. Box 6477 San Antonio, TX 78209
5	Brown University Division of Engineering ATTN: Prof. R. Clifton Prof. H. Kolsky Prof. L. B. Freund Prof. A. Needleman Prof. R. Asaro Providence, RI 02912
1	California Institute of Technology ATTN: T. J. Ahrens 1201 E. California Blvd. Pasadena, CA 91109

DISTRIBUTION LIST

No. of Copies	Organization
3	Carnegie-Mellon Universtiy Department of Mathematics ATTN: Dr. D. Owen Dr. M. E. Gurtin Dr. B. D. Coleman Pittsburgh, PA 15213
6	Cornell University Dept of Theoretical and Applied Mechanics ATTN: Dr. Y. H. Pao Dr. A. Ruoff Dr. J. Jenkins Dr. R. Lance Dr. F. Moon Dr. E. Hart Ithica, NY 14850
2	Denver Research Institute University of Denver ATTN: Mr. J. Wisotski Technical Library PO Box 10127 Denver, CO 80210
2	Harvard University Division of Engineering and Applied Physics ATTN: Prof. J. R. Rice Prof. J. Hutchinson Cambridge, MA 02138
2	Iowa State University Engineerng Research Lab ATTN: Dr. A. Sedov Dr. G. Nariboli Ames, IA 50010
5	The Johns Hopkins University ATTN: Prof. R. B. Pond, Sr. Prof. R. Green Prof. W. Sharp Prof. J. F. Bell Prof. C. Truesdell 34th and Charles Street Baltimore, MD 21218

No. of Copies	Organization
2	Lehigh University Center for the Application of Mathematics ATTN: Dr. R. Rivlin Dr. E. Varley Bethleham, PA 18015
1	Massachusetts Institute of Technology Aeroelastic and Structures Research Lab ATTN: Dr. E. A. Witmer Cambridge, MA 02139
1	Massachusetts Institute of Technology Mechanical Engineering Dept ATTN: Prof. K.-J. Bathe Cambridge, MA 02139
1	Massachusetts Institute of Technology ATTN: Technical Library Cambridge, MA 02139
1	Michigan Technological University Mechanical Engineering Dept ATTN: Prof. E. Chu Houghtom, MI 49931
1	New York University Dept of Mathematics ATTN: Dr. J. Keller University Height New York, NY 10053
1	North Carolina State University Dept of Civil Engineering ATTN: Prof. Y. Horie Raleigh, NC 27607
1	Northrop University ATTN: Dr. F. B. Safford 5800 W. Arbor Vitae St. Los Angeles, CA 90045

DISTRIBUTION LIST

No. of Copies	Organization
1	Pennsylvania State University Engineering Mechanics Dept ATTN: Prof. N. Davids University Park, PA 16502
3	Rensselaer Polytechnical Institute ATTN: Prof. E. H. Lee Prof. E. Krempl Prof. J. Flaherty Troy, NY 12181
1	Rice University ATTN: Dr. C. C. Wang P. O. Box 1892 Houston, TX 77001
1	Southern Methodist University Solid Mechanics Division ATTN: Prof. H. Watson Dallas, TX 75221
1	Stanford University Durand Laboratory ATTN: Dr. D. Bershader Stanford, CA 94305
1	Stevens Institute of Technology Dept of Mechanical Engineering ATTN: Prof. D. W. Nicholson Hoboken, NJ 07030
1	Temple University College of Engineering Technology ATTN: Dr. R. Haythornthwaite Dean Philadelphia , PA 19122
1	Tulane University Dept of Mechanical Engineering ATTN: Dr. S. Cowin New Orleans, LA 70112
3	University of California Dept of Engineering Mchanics ATTN: Dr. M. Carroll Dr. W. Goldsmith Dr. P. Naghdi Berkeley, CA 94704
1	University of California Dept of Aerospace and Mechanical Engineering Science ATTN: Dr. Y. C. Fung P. O. Box 109 La Jolla, CA 92037
1	University of California Dept of Mechanics ATTN: Dr. R. Stern 504 Hilgard Avenue Los Angele, CA 90024
1	University of California at Davis Dept of Engineering Science ATTN: Prof. Y. F. Dafalias Davis, CA 95616
1	University of California at Santa Barbara Dept of Mechanical Engineering ATTN: Prof. T. P. Mitchel Santa Barbara, CA 93106
1	University of California at Santa Barbara Dept of Material Science ATTN: Prof. A. G. Evans Santa Barbara, CA 93106
1	University of California at San Diego Dept of Mechanical Engineering ATTN: Prof. S. Nemat-Nassar La Jolla, CA 92093
2	University of Delaware Dept of Mechanical and and Aerospace Engineering ATTN: Dr. Minoru Taya Prof. J. Vinson Newark, DE 19711

DISTRIBUTION LIST

No. of Copies	Organization
4	University of Florida Dept of Engineering Science and Mechanics ATTN: Prof. L. Malvern Prof. D. Drucker Prof. E. Walsh Prof. M. Eisenberg Gainesville, FL 32601
2	University of Houston Dept of Mechanical Engineering ATTN: Dr. T. Wheeler Dr. R. Nachlinger Houston, TX 77004
2	University of Illinois Dept of Theoretical and Applied Mechanics ATTN: Dr. D. Carlson Prof. D. Scott Steward Urbana, IL 61801
2	University of Illinois at Chicago Circle College of Engineering Dept of Engineering, Mechanics, and Metallurgy ATTN: Prof. T. C. T. Ting Prof. D. Krajcinovic P. O. Box 4348 Chicago, IL 60680
2	University of Kentucky Dept of Engineering Mechanics ATTN: Dr. M. Beatty Prof. O. Dillon, Jr. Lexington, KY 40506
1	University of Kentucky School of Engineering ATTN: Dean R. M. Bowen Lexington, KY 40506
2	University of Maryland Dept of Mathematics ATTN: Prof. S. Antman Prof. T. P. Chou College Park, MD 20742

No. of Copies	Organization
3	University of Minnesota Dept of Engineering Mechanics ATTN: Prof. Y. L. Ericksen Prof. R. Fosdick Prof. R. James Minneapolis, MN 55455
1	University of Missouri-Rolla Dept of Engineering Mechanics ATTN: Prof. R. C. Batra Rolla, MO 65401-0249
2	University of Oklahoma School of Aerospace, Mechanical, and Nuclear Engineering ATTN: Prof. Akhar S. Khan Prof. Charles W. Bert Norman, OK 73019
1	University of Pennsylvania Towne School of Civil and Mechanical Engineering ATTN: Prof. Z. Hashin Philadelphia, PA 19105
4	University of Texas Dept of Mechanical Engineering ATTN: Dr. M. Stern Dr. M. Bedford Prof. Ripperger Dr. J. T. Oden Austin, TX 78712
1	University of Wasington Dept of Aeronautics and Astronautics ATTN: Dr. Ian M. Fyfe 206 Guggenheim Hall Seattle, WA 98195
1	University of Wyoming Dept of Mathematics ATTN: Prof. R. E. Ewing P. O. Box 3036 University Station Laramie, WY 82070

DISTRIBUTION LIST

No. of Copies	Organization
3	Washington State University Dept of Physics ATTN: Prof. R. Fowles Prof. G. Duvall Prof. Y. Gupta Pullman, WA 99163
2	Yale University ATTN: Dr. B.-T. Chu Dr. E. Onat 400 Temple Street New Haven, CT 96520

Aberdeen Proving Ground

Dir, USAMSAA
ATTN: AMXSY-D
AMXSY-MP, H. Cohen

Cdr, USATECOM
ATTN: AMSTE-SI-F

Cdr, CRDC, AMCCOM
ATTN: SMCCR-RSP-A
SMCCR-MU
SMCCR-SPS-IL

USER EVALUATION SHEET/CHANGE OF ADDRESS

This Laboratory undertakes a continuing effort to improve the quality of the reports it publishes. Your comments/answers to the items/questions below will aid us in our efforts.

1. BRL Report Number ______________________ Date of Report ____________

2. Date Report Received ____

3. Does this report satisfy a need? (Comment on purpose, related project, or other area of interest for which the report will be used.) ____________

4. How specifically, is the report being used? (Information source, design data, procedure, source of ideas, etc.) ____________

5. Has the information in this report led to any quantitative savings as far as man-hours or dollars saved, operating costs avoided or efficiencies achieved, etc? If so, please elaborate. ____________

6. General Comments. What do you think should be changed to improve future reports? (Indicate changes to organization, technical content, format, etc.)

CURRENT ADDRESS

Name

Organization

Address

City, State, Zip

7. If indicating a Change of Address or Address Correction, please provide the New or Correct Address in Block 6 above and the Old or Incorrect address below.

OLD ADDRESS

Name

Organization

Address

City, State, Zip

(Remove this sheet, fold as indicated, staple or tape closed, and mail.)

FOLD HERE

Director
US Army Ballistic Research Laboratory
ATTN: DRXBR-OD-ST
Aberdeen Proving Ground, MD 21005-5066

NO POSTAGE NECESSARY IF MAILED IN THE UNITED STATES

OFFICIAL BUSINESS
PENALTY FOR PRIVATE USE, $300

BUSINESS REPLY MAIL
FIRST CLASS PERMIT NO 12062 WASHINGTON, DC

POSTAGE WILL BE PAID BY DEPARTMENT OF THE ARMY

Director
US Army Ballistic Research Laboratory
ATTN: DRXBR-OD-ST
Aberdeen Proving Ground, MD 21005-9989

FOLD HERE